Key Points:

- A reconstruction of past millennium hurricane activity from Long Island in The Bahamas conflicts with records from neighboring islands
- Storm properties, local hydrodynamics, and the depositional environment are important for storm deposition at a blue hole site
- Compilations of Atlantic paleohurricane records indicate century-scale shifts in regional storm population over the past 1,000 years

1,050 years of Hurricane Strikes on Long Island in The Bahamas

E. J. Wallace[1], J. P. Donnelly[2], P. J. van Hengstum[3,4], T. S. Winkler[4], K. McKeon[5,2], D. MacDonald[5], N. E. d'Entremont[2], R. M. Sullivan[4], J. D. Woodruff[5], A. D. Hawkes[6], and C. Maio[7]

[1]Massachusetts Institute of Technology/Woods Hole Oceanographic Institution Joint Program in Oceanography, Woods Hole, MA, USA, [2]Department of Geology and Geophysics, Woods Hole Oceanographic Institution, Woods Hole, MA, USA, [3]Department of Marine Sciences, Texas A&M University at Galveston, Galveston, TX, USA, [4]Department of Oceanography, Texas A&M University, College Station, TX, USA, [5]Department of Geosciences, University of Massachusetts Amherst, Amherst, MA, USA, [6]Department of Earth and Ocean Sciences, Center for Marine Sciences, University of North Carolina Wilmington, Wilmington, NC, USA, [7]Department of Geosciences, University of Alaska Fairbanks, Fairbanks, AK 99775, USA

Abstract Sedimentary records of past hurricane activity indicate centennial-scale periods over the past millennium with elevated hurricane activity. The search for the underlying mechanism behind these active hurricane periods is confounded by regional variations in their timing. Here, we present a new high resolution paleohurricane record from The Bahamas with a synthesis of published North Atlantic records over the past millennium. We reconstruct hurricane strikes over the past 1,050 years in sediment cores from a blue hole on Long Island in The Bahamas. Coarse-grained deposits in these cores date to the close passage of seven hurricanes over the historical interval. We find that the intensity and angle of approach of these historical storms plays an important role in inducing storm surge near the site. Our new record indicates four active hurricane periods on Long Island that conflict with published records on neighboring islands (Andros and Abaco Island). We demonstrate these three islands do not sample the same storms despite their proximity, and we compile these reconstructions together to create the first regional compilation of annually resolved paleohurricane records in The Bahamas. Integrating our Bahamian compilation with compiled records from the U.S. coastline indicates basin-wide increased storminess during the Medieval Warm Period. Afterward, the hurricane patterns in our Bahamian compilation match those reconstructed along the U.S. East Coast but not in the northeastern Gulf of Mexico. This disconnect may result from shifts in local environmental conditions in the North Atlantic or shifts in hurricane populations from straight-moving to recurving storms over the past millennium.

1. Introduction

The past three Atlantic hurricane seasons (2017–2019) have collectively caused ~330 billion USD in damages and a death toll of >3,000 people (Cangialosi et al., 2018; Kishore et al., 2018; Pasch et al., 2019). The massive damage associated with these recent storms is in large part due to the increase in coastal population and infrastructure over the past century (Mendelsohn et al., 2012; Pielke et al., 2008). This increasing coastal wealth in concert with rising sea levels has amplified coastal vulnerability to storm inundation (Woodruff et al., 2013). In addition, a growing body of climatological research suggests that global warming will produce stronger hurricanes (Bhatia et al., 2018; Emanuel, 2013; Korty et al., 2017; Sobel et al., 2016; Walsh et al., 2016; Zhang et al., 2017). It is difficult to put these projections into a broader historical context given the short nature of the observational record of hurricane activity (Knutson et al., 2019). With only 169 years of observations in the Atlantic (NOAA Best Track-Knapp et al., 2010), we cannot rigorously separate concurrent natural and anthropogenic influences on hurricane frequency nor can we assess how hurricanes and climate interact on multi-decadal to centennial timescales.

Fortunately, hurricanes, particularly more intense storms, leave behind distinct coarse-grained sediment layers in coastal basins that allow us to track storm landfalls deeper back in time (Wallace et al., 2014). In particular, sediment cores collected from coastal ponds (e.g., Bregy et al., 2018; Donnelly et al., 2015; Donnelly & Woodruff, 2007) and marshes (e.g., Boldt et al., 2010; McCloskey & Liu, 2012) have faithful-

ly documented local hurricane passages over hundreds to even thousands of years. Many of these paleo-hurricane reconstructions indicate that periods of historically unprecedented levels of intense hurricane activity in the Atlantic occurred over the past millennium. Recent work has shown that sediment records from coastal karst basins (CKBs), such as fully submerged blue holes (e.g., Schmitt et al., 2020; Wallace et al., 2019; Winkler et al., 2020) and sub-aerial sink holes (e.g., Brandon et al., 2013; Brown et al., 2014; Lane et al., 2011; van Hengstum et al., 2016), can provide high resolution records of paleohurricane strikes. CKBs are basin-like features that form through dissolution processes on carbonate platforms (Mylroie et al., 1995; van Hengstum et al., 2011) and are scattered across the hurricane-prone tropical Atlantic. Despite their suitability for paleohurricane research and their prevalence in the tropics, there are currently relatively few reconstructions from these basins.

Recent studies confirm the utility of blue hole sediment cores in reconstructing hurricane activity over the past two millennia (Denommee et al., 2014; Schmitt et al., 2020; van Hengstum et al., 2014; Wallace et al., 2019; Winkler et al., 2020). All of these blue hole records contain coarse-grained event deposits that correlate with known historical hurricane strikes, have near-annual resolution, and show prolonged periods of both elevated and reduced hurricane activity. Winkler et al. (2020) updates previous work from Thatchpoint Blue Hole on Abaco Island in The Bahamas (van Hengstum et al., 2014) documenting local hurricane strikes on the island over the past 700 years. Schmitt et al. (2020) and Wallace et al. (2019) present longer records documenting hurricane strikes over the past 1,500 years from Lighthouse Reef blue hole in Belize and South Andros Island in The Bahamas, respectively. Both of these studies suggest that active and inactive periods of hurricane activity occur coeval with shifts in hemispheric-scale oceanic and atmospheric climate features such as the Intertropical Convergence Zone (ITCZ) and the North Atlantic Oscillation (NAO; Denommee et al., 2014; Schmitt et al., 2020; Wallace et al., 2019).

When comparing the Caribbean records to records from the U.S. mainland coastline, there is clear regional variation in the timing of these active and quiet intervals. Wallace et al. (2019) noted that the South Andros record showed similar patterns of activity to records from the Florida Gulf Coast (Brandon et al., 2013; Lane et al., 2011) but directly contrasted with a record from Salt Pond in Massachusetts (Donnelly et al., 2015). In particular, the records from the Gulf Coast and South Andros showed high activity from 1100 CE to the mid-fifteenth century but were relatively quiet from 1450–1650 CE when Salt Pond was active. The authors suggested that this shift in tracks was likely tied either to changes in local environmental conditions or climate driven geographic variability in hurricane tracks and intensity (Wallace et al., 2019). This is all confounded by the inherent stochasticity associated with hurricane landfalls (i.e., hurricanes might strike one sample location more frequently than others over a time period simply as a result of randomness).

To solve this puzzle, we need more paleohurricane proxies throughout the Caribbean to better constrain how storm activity shifted from lower latitudes to the U.S. coastline. There are no other records from The Bahamas that compare in length or resolution to the record on South Andros Island. The recently updated record from Thatchpoint Blue Hole on Abaco Island, The Bahamas (Winkler et al., 2020), provides similar resolution (~near-annual) to South Andros but only extends back ~700 years. Therefore, it is crucial to acquire more high resolution records of the past millennium to assess the regional coherency of storm frequency in The Bahamas.

In tandem with the uncertainties in the climatic interpretations of these blue holes are further unknowns about the sedimentary processes that are at play in blue hole environments during hurricanes. Our assumption is that during storm events storm surge and waves at the surface induce strong bottom currents which suspend and transport sediment into the blue hole (Miller et al., 1977). However, this explanation does not account for complicated sedimentary processes at play on carbonate platforms during storm events. Blue hole sites in tidal channels (Wallace et al., 2019) and deeper water (Schmitt et al., 2020; Winkler et al., 2020) preserve stratigraphic records of storm passages while more sheltered sites surrounded by supratidal islands (van Hengstum et al., 2020) do not. The sensitivity of each blue hole site to hurricane event bed deposition is likely influenced by its proximity to different tidal channels, shielding by local topography, and local sediment characteristics. We need more information about the processes dictating sedimentation in blue hole systems to aid in interpreting current and future paleohurricane records.

Unfortunately, it is prohibitively dangerous to observe blue hole sites during intense hurricane strikes and the destructive nature of hurricanes usually results in damaged or lost instrumentation and sensors. These difficulties are all exacerbated by the irregularity in which a hurricane makes landfall near these sites. It is often difficult even to use the observational record of storms (1850-present) to uncover what types of hurricanes leave deposits. Since storms frequently impact sites in the Caribbean, age uncertainties associated with each event deposit make it difficult to unequivocally link a particular storm event to a respective deposit.

Generally, historical attribution within sedimentary archives reveals that the close passage of an intense storm is often the source of easily distinguished event beds at a site. In the South Andros Island record (Wallace et al., 2019), the authors argued that the two modern event deposits corresponded to the proximal passage of Category 3 hurricanes in 1945 and 1919. However, the most important metric for determining storm surge and coarse-grained sediment transport are not the individual properties of the storm itself but instead the local flood and transport conditions induced by that storm's passage. Different local characteristics (e.g., sources/sinks of sediment; location of geomorphic features, coastline geometry) can dramatically impact whether a site deposits and preserves an event bed. On South Andros, sediment cores from a different blue hole located only a few kilometers away from the primary record presented by Wallace et al. (2019) did not capture coarse deposits during the 1945 and 1919 hurricanes. Hydrodynamic modeling work (Lin et al., 2014) on barrier beach environments in Northwest Florida shows that a wide range of storm characteristics (intensity, duration, track, size) can all result in sufficient storm surges to overtop coastal barriers and leave event deposits in a coastal lagoon. To fully understand the distribution of storm intensities that leave a deposit at a blue hole site, we need reliable simulations of the local conditions near a blue hole and/or actual wave, water level, and current observations.

In this study, we present a high resolution record of event bed frequency in a blue hole off the west coast of Long Island, The Bahamas. The record spans the past 1,050 years and contains seven event beds which temporally correlate to seven Category 2 and above hurricanes that passed over the site since 1850 CE. These historical tempestites give us the opportunity to investigate how modern events of a known character leave deposits in blue holes. We also present current speed and direction data measured during the distant passage of Hurricane Irma in 2017. With its position close to records from South Andros (Wallace et al., 2019) and Abaco Island in The Bahamas (van Hengstum et al, 2014, 2016; Winkler et al., 2020), this site offers the perfect opportunity to assess the regional coherency of storm frequency in The Bahamas. We use this record to evaluate the temporal variability of hurricane strikes on Long Island and combined with other available reconstructions we assess geographic variability of hurricane strikes along the U.S. coastline and throughout the tropical Atlantic.

2. Methods

2.1. Study Site

Long Island is situated on the eastern margin of the Great Bahama Bank in the central Bahamas. It lies 265 km east of the location of the South Andros Island reconstruction (Wallace et al., 2019) and 400 km to the southeast of the location of reconstructions from Abaco Island (van Hengstum et al., 2016; Winkler et al., 2020). These records provide an established geographic context in which to compare our reconstruction and offer an opportunity to test variability in hurricane tracks.

We collected cores in April 2016 from a blue hole in the subtidal carbonate lagoon off the northwest shore of Long Island (23.265°N, 75.117°W). The blue hole is situated approximately 400 m from the coast (Figure 1b), and the L-shaped geometry of Long Island's northwest shore promotes greater onshore-directed waves and surge at the site from southeast-directed winds. The blue hole is approximately 150 m in diameter with a maximum depth of 12 m (Figure 1c). In April, CTD casts taken from the center of the blue hole indicate warmer temperatures (~27°C) in the top 2 meters followed by a gradual thermocline to cooler waters (~24.5°C) from 6 m to the bottom of the hole (Figure S1). The temperature profile in January of 2017, on the other hand, suggests a collapsed thermocline in the winter months with much cooler temperatures (~24°C) at surface (Figure S1). The water depth surrounding the hole is 1–2 m deep.
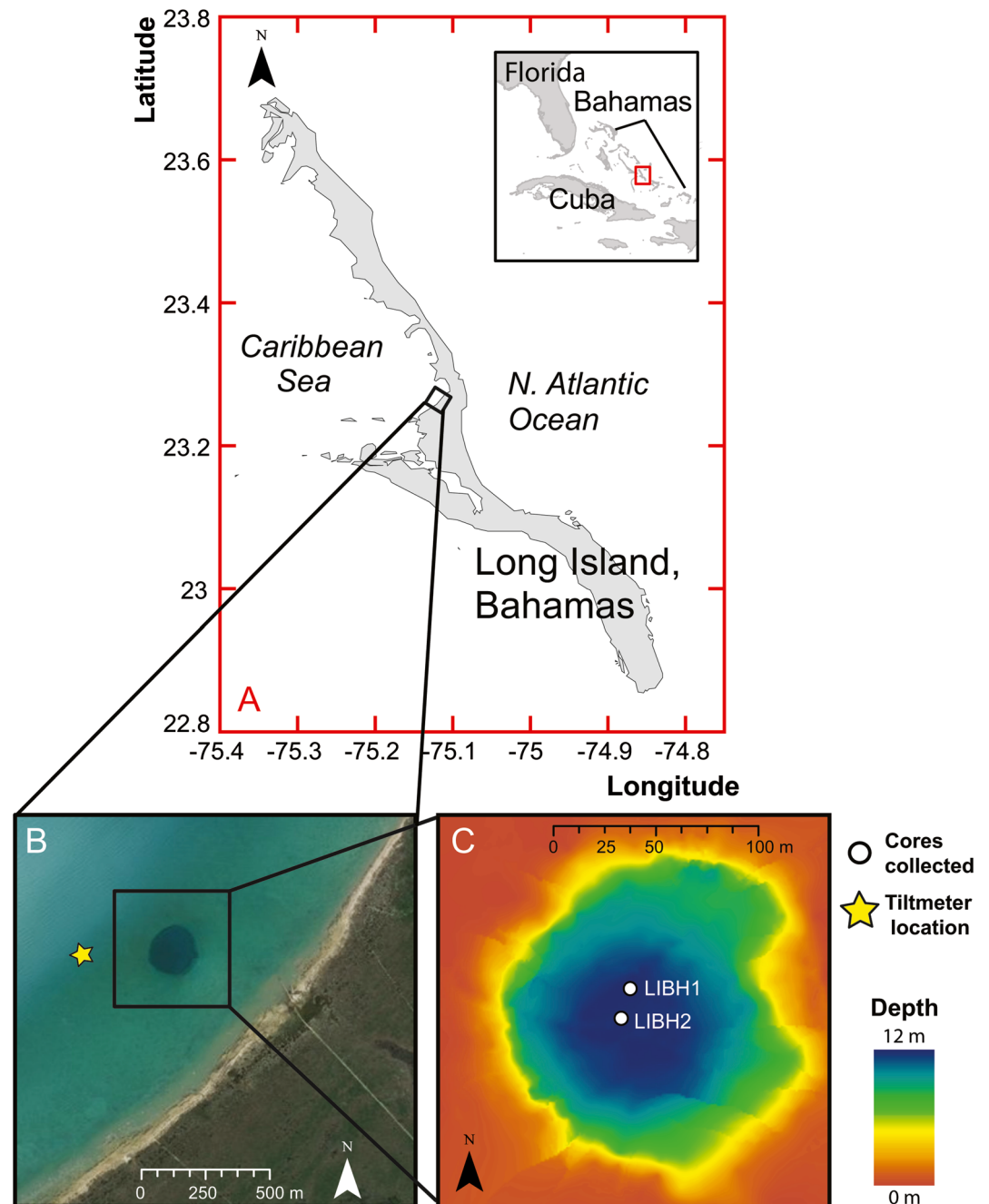
Figure 1. (a) Map of Long Island, The Bahamas. (b) Long Island Blue Hole (LIBH) location (23.265°N, 75.117°W), (c) The bathymetry of the blue hole and locations of the two cores (LIBH1 and LIBH2) are shown. The location of the tiltmeter we deployed in January 2017 is indicated by the yellow star in (b). LIBH, Long Island Blue Hole.

Long Island is positioned along the trackway of many hurricanes originating in the Caribbean and Atlantic. Multiple intense hurricanes passed the island in recent years. In 2015, the year before the cores were taken, the center of circulation of Hurricane Joaquin passed 40 km east of the blue hole at Category 4 strength. Months after coring, Hurricane Matthew passed 100 km to the southwest of the site at Category 3 strength in September 2016. Hurricane Irma in 2017 passed much further away (∼200 km) to the southwest of the blue hole also at Category 4 strength.
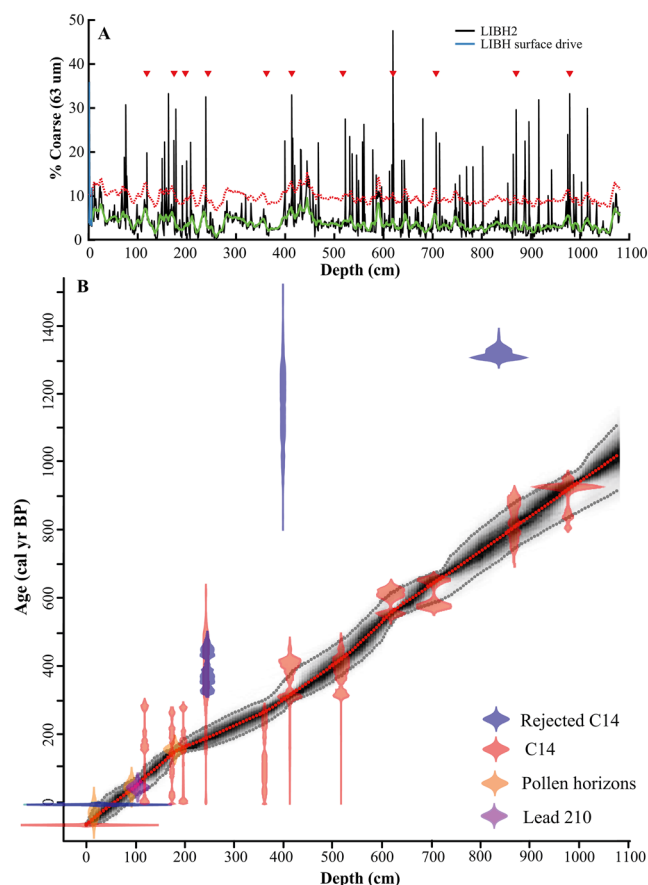
Figure 2. (a) Percent sand fraction (>63 μm) versus depth in core (black) from LIBH2 with a 10-point running mean filter (green) that excludes coarse fraction values above 10%. The first 8 cm are drawn from the LIBH surface drive (blue). The red dashed line is the event cutoff threshold added to the filter. Location of ^{14}C dates are plotted as red triangles above the coarse fraction data. Event beds are shown as a single cm peak. (b) Age model (red dashed) derived from radiocarbon dates (red) in Table S2, pollen horizons (orange) from smear slides in Table S1, and dated onset of detectible unsupported Lead 210 (purple; profile in Figure S3) for LIBH2. 95% confidence bounds are shaded in gray around the age model. A tie point setting the surface of each core to modern is also shown (red horizontal bar). Rejected dates are shown in blue. These figures were generated using BACON v2.2 age modeling software (Blaauw & Christen, 2011). BACON, Bayesian accumulation histories for deposits; LIBH, Long Island Blue Hole.

2.2. Field Methods

We cored the blue hole using a Rossfelder P-3 vibracore from the *RV Arenaria*, a customized 6-m pontoon vessel. The *Arenaria*, personnel, and equipment were transported to Long Island aboard the *MV Alucia* and field operations were supported by the *Alucia's* tender the *Northwind*. We collected two long neighboring vibracores LIBH1 (~8 m) and LIBH2 (~11.5 m) from the center of the blue hole. Both LIBH1 and LIBH2 do not contain the sediment water interface. Therefore, we collected a short surface core (LIBH1 D2) in which we carefully curated the core top. The first 28 cm of the LIBH2 record stems from this surface core which contains an event layer (likely from Hurricane Joaquin) within the first 2 cm. We stratigraphically linked the surface core and longer drive (LIBH2) by matching the coarse fraction data from both cores (Figure S2).

In January 2017, we returned to the site and took two short surface grabs (~5 cm) to capture any sediments potentially deposited from Hurricane Matthew in 2016. We also deployed a Lowell Instruments LLC Tilt Current Meter (TCM) approximately 30 m to the northwest of the hole in 1.5 m of water (Figure 1). This sensor measures bottom current speed and direction as well as temperature. It was recovered in 2018 and captured data during the passage of Hurricane Irma on September 8–10, 2017.

2.3. Sediment Analysis and Age Control

Following the procedures of Wallace et al. (2019), we sampled the LIBH1 and LIBH2 cores continuously at 1 cm intervals, dried subsamples for 8 h in 100°C and wet sieved them at 63 μm. We dried and weighed the residual to determine its coarse fraction by dry weight. Most chronological control for the longer LIBH2 core was based on radiocarbon dates. However, we also include chronostratigraphic ages from pollen derived evidence of known land use changes and Pb-210 radionuclide activity over the last few centuries into our age model.

Fossil pollen records can document changes in terrestrial flora that can be used as chronological tie points. We established three control points in the top 200 cm of LIBH2 from pollen horizons in smear slides from 10 different samples from LIBH2 (Table S1). Smear slides provide semi-quantitative compositional information which we used to determine the presence and absence of pollen taxa in sedimentary units in LIBH2 without detailed pollen analysis. Vegetation nomenclature follows Correll and Correll (1982). The furthest downcore samples (233 and 286 cm) indicate that Long Island was dominated by dry tropical hardwood coppice forest with some palms and no agricultural disturbances on the landscape. At both 181 and 198 cm, the pollen in the smear slides start to indicate disturbance in the environment including weedy disturbance taxa like Asteraceae (i.e., Genera *Ambrosia* and *Conyza*; Correll & Correll, 1982). In particular, the sample at 193 cm contains macro-charcoal fragments with nearly all of the coppice pollen taxa absent. This interval is likely associated with the extensive plantation at Gray's Settlement (1784–1814 CE), one of some 4,000 acres of cotton plantations on Long Island (Craton & Saunders, 1992; Eneas, 1998). We assign the age of the onset of cotton agriculture at 193 cm to 1795 ± 10 CE. This tie point is consistent with an independent radiocarbon date at 181 cm (Table S2 and Figure 2).

The smear slide at 98 cm also indicated taxa associated with scattered forest disturbance and sisal cultivation including Agavaceae (cf. *Agave sisalana*; Table S1). In 1890 CE, The Bahamas had some 100,000 acres in sisal production and Long Island cultivated approximately 250 acres of sisal in 1908 (Craton, 1968;
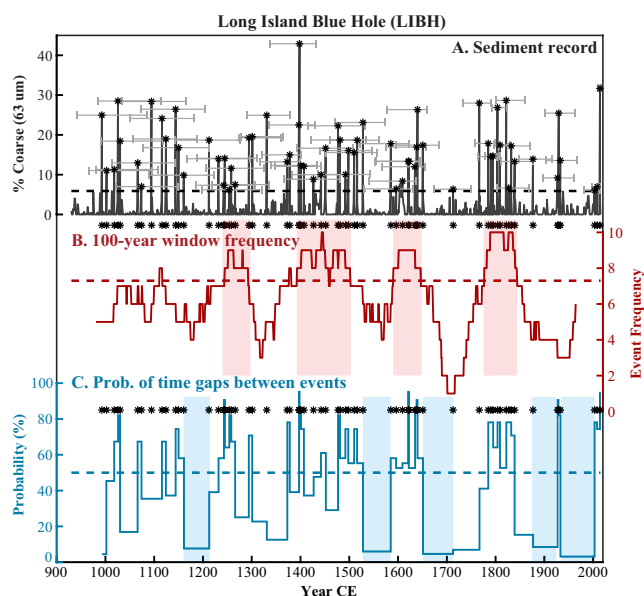
Figure 3. (a) Coarse anomaly plot (solid line) for LIBH2 as a function of time. The dashed black line is the event bed threshold of 5.90%. Gray error bars indicate 95% confidence bounds for the ages of each event. (b) The 100-year moving window event frequency per century. The dashed red line is the regional cutoff for active intervals (7.3 events/century). (c) The probabilities of having no events over the time span between each event in the record. The dashed blue line indicates the 50% cutoff line. The probabilities were calculated based on a recurrence interval of 16.4 years/event over the whole record (blue). Active and quiet intervals identified on Long Island are shaded in red and blue, respectively. LIBH, Long Island Blue Hole.

Eneas, 1998; Little et al., 1977). The Bahamas experienced a sisal production boom in 1916 CE during World War I, and ending in 1920 CE (Eneas, 1998). Thus, we assign the age of the sample from 98 cm to within the sisal period on Long Island (1905 ± 15 CE). The two top most smear slides (18 and 40 cm) indicate a return to the coppice forest matrix with either small farm clearings or no disturbance taxa (Table S1). At 40 cm, the presence of the popular agriculture trees (e.g., the hog plum, *Spondias*) and opaque spherules (indicating fossil fuel combustion) document some human presence on the landscape (Clark & Patterson, 1984; Griffin & Goldberg, 1975). Spherules are sparsely evident in the sample from 18 cm likely reflecting the population loss and loss of farm sites on Long Island around 1943 CE and continuing through 1960 CE (Craton & Saunders, 1998). Thus, we interpret the age at 18 cm to be 1980 ± 20 CE.

We measured Lead 210 (^{210}Pb) on bulk sediment samples in top 170 cm of the LIBH surface drive on Canberra GL2020RS low-energy Germanium gamma well detectors. We used the Constant Rate of Supply (CRS) model (Appleby, 2001; Appleby & Oldfield, 1978) to identify and date the ^{210}Pb equilibrium line (Figure S3) at 110 cm to 1906 ± 10 CE. This ^{210}Pb control point is consistent with the pollen horizon for sisal cultivation on Long Island at 101 cm (Figure 2).

We use 11 radiocarbon dates from LIBH2 to establish age control through the rest of the core (Figure 2 and Table S2). All dates were derived from mangrove leaves and plant matter preserved in the cores. They were dated at the National Ocean Sciences Accelerator Mass Spectrometry facility in Woods Hole, MA. We used Bayesian accumulation histories for deposits (BACON) software v2.2 to create the age model (Blaauw & Christen, 2011). Radiocarbon dates were calibrated using IntCal13 and postbomb radiocarbon was calibrated with CALIbomb under the compiled Northern Hemisphere Zone 2 data set (Reimer et al., 2004). We excluded five dates from the chronology (Figure 2 and Table S3) as they were not chronologically consistent with younger dates obtained at a similar depth. These samples likely indicate older reworked material from the landscape (Supporting Information). Throughout the record, we assume event beds are deposited in hours. Thus, we condense all event beds down to 1 cm, remove them for age-depth modeling, and then reinsert them as instantaneous events.

2.4. Event Threshold, Attribution, and Frequency

Event beds in the core were identified predominantly using the coarse fraction data. We followed the methods of Donnelly et al. (2015) and Wallace et al. (2019) to create an event bed cutoff threshold for the coarse fraction data. We calculated the coarse anomaly by removing a 10-point moving average from the coarse fraction data. This filter did not include coarse fraction peaks over 10% to prevent larger peaks skewing the filter and leading to exclusion of neighboring smaller peaks. Event beds are coarse anomaly peaks that exceed two sigma (95%) of the cumulative distribution function of the coarse anomaly data from 1851 to present. The threshold for LIBH is 5.9%.

We confirmed our choice of event bed cutoff by cross-checking coarse anomaly peaks marked as event beds against the location of visible event beds in the cores. All visible event beds corresponded to a peak in the coarse fraction data. Common visual indicators of event beds include: higher concentrations of organic matter throughout the deposit, visibly coarser grains and lighter colored sediments. We calculated event frequency per century by counting up the number of events in 100-year (Figure 3) and 50-year moving windows (Figure S4). The 100-year window emphasizes centennial scale comparisons within the record while the 50-year window shows multi-decadal shifts in events.

2.5. Defining Active and Quiet Intervals

We calculated the expected event frequency (λ) for the Long Island blue hole (LIBH) using the regional estimate method detailed in Wallace et al. (2019) and used by Winkler et al. (2020) for Category 2 and above storms. See Section 4.1 for a justification of our choice of storm intensity thresholds for Long Island. This method calculates an expected event frequency for the northern Caribbean from Turks and Caicos up to Grand Bahama using storms in the Best Track data set (1851–2016 CE). The expected frequency estimate for Category 2 and above hurricanes calculated using this method is 3.7 events/century. We can calculate an upper confidence bound on this expected event frequency estimate by treating a storm's arrival to the site as a Poisson process. We computed a 95th percentile solution (Ulm, 1990), yielding a value of 7.3 events/century. Any activity exceeding this 95% bound is outside what it is expected based on random variations of hurricane frequency over past 158 years. Thus, we define active intervals as periods of time when the 100-year window event frequency was above this 95th percentile solution (7.3 events/century) or essentially above what we expect given historical levels of hurricane activity in the northern Caribbean (Figure 3).

Quiet intervals were also defined using the same procedures as Wallace et al. (2019). The recurrence interval (T) was set at 16.4 years/event based on the 66 hurricanes that passed the blue hole over the entire record (930–2016 CE). The probability of having no events (PT) for r number of years in the record was calculated using Equation 1.

$$P_T = \left(1 - \frac{1}{T}\right)^r \qquad (1)$$

Extended periods of time (>50 years) when PT was below 50% were counted as quiet intervals (Figure 3).

2.6. Estimating Storm Surge Using SLOSH

We simulated max storm surge for every historical hurricane (Saffir Simpson Category 1 and above) that passed within 100 km of LIBH using the SLOSH (Sea, Lake, and Overland Surges from Hurricanes) model from the National Weather Service (Jelesnianski et al., 1992). Blue hole environments, like the one on Long Island, are generally susceptible to storms passing closer than 100 km from the site and at hurricane strength or higher (Denommee et al., 2014; Schmitt et al., 2020; Wallace et al., 2019; Winkler et al., 2020). SLOSH is a low-resolution numerical model that applies the wind and pressure fields from storms together with a digital elevation model of the coastline to simulate storm surges. SLOSH is divided up into a number of polar, hyperbolic, and elliptical grids. It includes parameterizations for some sub-grid features like variable friction from vegetation, channel flow, and barriers to flow. We used the only SLOSH simulation grid that encompasses Long Island: Bahamas (basin code: andrwnhc.bha). This grid is coarsely resolved near Long Island with ~5 km by 5 km grid cells. Therefore, we expect SLOSH storm surge estimates for Long Island to be rough estimates of max storm surge at our site. Although, in comparison to other higher resolution models, SLOSH has been found to capture max storm surge pretty well for areas with simple coastal features (Lin et al., 2010). We used the SLOSH estimates for storm surge for each modern storm to help determine which of these storms likely contributed to event beds found in our cores (See Section 4.1).

3. Results

3.1. Event Bed Description

The Long Island blue hole sediment cores (LIBH1, 775 cm and LIBH2, 1,148 cm) contain predominantly fine-grained carbonate mud with scattered coarser layers ranging from very fine sand (0.088–0.125 mm) to very coarse sand (1.41–2 mm). The sediment stratigraphy is dominated by pale brown colored (Munsell color 2.5Y 6–3) sediment with gray (Munsell color 2.5Y 7–1) and white (Munsell color 7.5Y 8–1) laminations. There is no evidence of bioturbation in the cores. The LIBH sediment record exhibits an average sedimentation rate of 1.1 cm/yr (ranging from 0.6 to 2.5 cm/yr) for the full 1,148 cm LIBH2 core. This gives our record near annual resolution with each single cm sample representing approximately one year of sedimentation.

We identified 66 event beds in the LIBH2 record over the past 1,050 years. Thus, the average event frequency on Long Island is 6.2 events/century. In most cases, these event beds stand out with visibly coarser grains, white and gray colors, and/or higher concentrations of plant matter. Quantitatively, event beds stand out in the coarse fraction data with values ranging from 10% to 48% sand and gravel (i.e., >63 μm). A vast majority of the event beds (63 of 66) are 1–3 cm thick. We did not find evidence of event beds or coarser sediment in the surface grabs from Long Island taken in 2017 after Hurricane Matthew's passage in October 2016 to the south.

We correlated the stratigraphy for LIBH2 and LIBH1 for the overlapping top ~800 cm (Figure S5). Nearly all of the same event beds were identified in the neighboring shorter core (LIBH1; Figure 1). Over the top 800 cm, we identified 45 events in LIBH2 and 42 events in LIBH1.

3.2. Changing Event Frequency

Over the past 1,050 years, there have been extended periods (>50 years) with frequent events occurring on Long Island. We define four active intervals on Long Island using the 100-year window event frequency from 1245–1290 CE, 1395–1500 CE, 1590–1650 CE, and 1775–1845 CE (Figure 3). Of these active intervals, the period with the most events is the most recent active interval from 1775–1845 CE with an average event frequency of 9.3 events/century. The timing of these four active intervals is confirmed in the 50-year window event frequency data. The 50-year window event frequency emphasizes the multi-decadal periods with the highest activity. Long Island experienced five exceptionally active intervals from 1229–1267 CE, 1376–1422 CE, 1485–1516 CE, 1597–1647 CE, and 1780–1835 CE with over 10 events/century, almost double the average event frequency in the whole record (Figure S4).

Interspersed between these active intervals are periods with really low event frequency. We define these quiet intervals as periods extending longer than 50 years in which there are zero events beds and the probability of having zero events is below 50%. According to these criteria, the west coast of Long Island was relatively quiet from 1161–1213 CE, 1528–1585 CE, 1651–1713 CE, 1877–1927 CE, and 1933–2003 CE (Figure 3).

3.3. Irma 2017 Tilt Current Meter (TCM) Data

The tiltmeter data from Long Island includes the entirety of September 2017. From this data, we gain an understanding of the average bottom current conditions in the lagoon nearby the blue hole and how the passage of distant storms changes the hydrodynamics. We compare storm current direction and speed during Hurricane Irma (September 7–11, 2017) and Hurricane Maria (September 21–25, 2017) to ambient conditions (September 1–4, 2017). Under ambient conditions in September, current direction was predominantly to the northwest (Figure 4b). Bottom velocity varied on an approximately 12-h cycle with the tides from low values at ~0.01 m/s at high and low tide to peak values at ~0.025 m/s midway between high and low tide.

Hurricane Irma 2017 passed 200 km to southeast of LIBH (Figure S6), but its effects on the island were still significant in terms of both the winds and waves. Videos (https://time.com/4935096/long-island-bahamas-irma-hurricane/) and eye-witness accounts from the storm suggest that Irma's passage caused drainage of water off the Great Bahama Bank, which caused a decrease in water depth to the carbonate lagoon on the western periphery of Long Island. This is not an uncommon occurrence in The Bahamas (Neely, 2013). The high winds and low-pressure center accompanying a hurricane siphon water off carbonate banks in The Bahamas and pile it nearer to the center of the storm. After the storm's passage, this water flows back onto the bank. In the case of Irma, water was pulled off places like Long Island, Exuma Island, Acklins Island, and Tampa Bay and transferred to increase water elevations in the Gulf of Mexico (https://www.theatlantic.com/science/archive/2017/09/irma-sucks/539325/).

Our tiltmeter data confirms eye-witness accounts, documenting a 6-h period of time during the peak of Irma's passage when the tiltmeter was lying on its side presumably on dry ground (Figure 4). The accelerometer data indicates that the tiltmeter began to go aground starting on September 8th at ~10 a.m. as the water started to drain from the carbonate lagoon surrounding LIBH (Figure S7). By ~1 p.m., it was fully on its side. It remained this way for 6 h before it started to float again around ~7 p.m. as the water returned to the area. We also observed a complete change in current direction before and after the storm (Figure 4c).
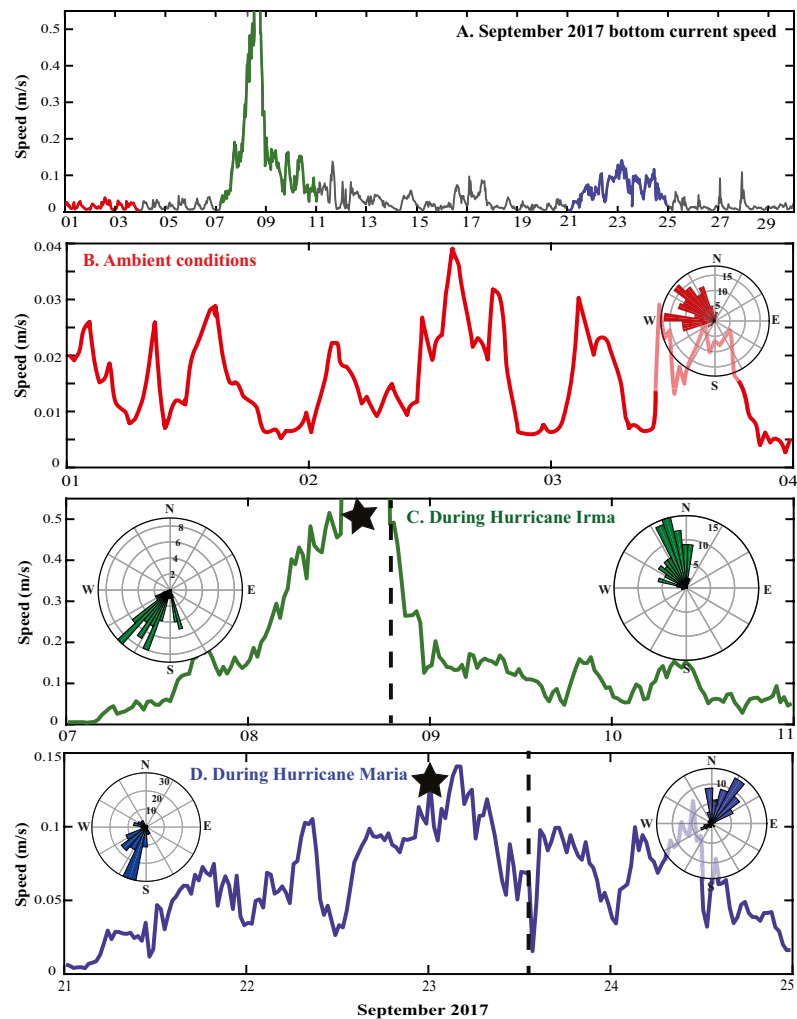
Figure 4. Bottom current speeds in September 2017 (a), under ambient conditions (September 1–4, 2017) (b), during Hurricane Irma (September 7–11, 2017) (c), during Hurricane Maria (September 21–25, 2017) (d). All data was taken from a Lowell Instruments LLC Tilt Current Meter (TCM) logging at a burst interval of 2 min, a burst rate of 8 Hz, and a burst duration of 30 s. There is no data during the peak of Irma's passage, because water drained from the lagoon. Rose plots of current direction are shown in each panel. In (c) and (d), we display current direction from before and after each storm. The dashed back lines denote our definition of the split between before and after each storm. The black stars denote the time of closest passage for Irma (c) and Maria (d). TCM, Tilt Current Meter.

Current direction at the beginning of Irma was oriented predominantly to the southwest. In contrast, for the later stages of the storm, current direction switched back to the northwest. This change in current direction also provides further evidence for the lagoon draining. During the peak of Irma, water was siphoned from the lagoon near LIBH toward the storm to the southwest and returned 6 h later, flowing to the northwest.

Unfortunately, we cannot tell whether or not the bottom current created from water draining off or returning to the lagoon during Irma was strong enough to transport sediment. The current speed rose to approximately 0.5 m/s before water started draining from the lagoon and compromised the tiltmeter measurements (Figure 4). This is much lower than the current speed of 2 m/s simulated by Sahoo et al. (2019) for Hurricane Joaquin. Bottom currents four times smaller during Irma than Joaquin are consistent with the lack of an Irma deposit supporting the notion that currents generated during this storm were insufficient to suspended coarse sediment significantly on the western Long Island lagoon.

Hurricane Maria passed too far away (>350 km) to drain the water from the west coast of Long Island. Our tiltmeter continued to collect data throughout the storm and we observe a change in current direction

during Maria (Figure 4d). Maria passed by Long Island to the east. South to southwest winds in the top left quadrant of the storm likely created the southwest current we observed on Long Island during the beginning of Maria's passage. The switch in current direction to the northeast after Maria's passage captures the return flow to the lagoon. We also observed a drop in water temperature around the blue hole as both Irma and Maria passed (Supporting Information, Section 2, and Figure S8).

Comparing storm condition current speeds (both measured and simulated) to the observed ambient conditions near the LIBH highlight the potential for storms to dramatically alter the hydrodynamics on shallow carbonate lagoons. Under ambient conditions, the highest bottom current speed we observed in 2017 was ~0.025 m/s. This is over an order of magnitude lower that the current speeds observed during the very distal passages of Hurricane Irma and Hurricane Maria in September 2017 to the south and northeast of the island, respectively. During these storms, we recorded current speeds near LIBH ranging from 0.1 to 0.5 m/s. Meanwhile, simulations of close-moving storms like Hurricane Joaquin in 2015 generate bottom currents on the west coast of Long Island at around 2 m/s (Sahoo et al., 2019), two orders of magnitude higher than we observed for ambient conditions and one order higher than observed for the passage of distant storms like Hurricane Maria and Irma. Hurricane Irma and Maria likely did not leave coarse deposits in LIBH, but Hurricane Joaquin did. From this, we can narrow down the range of bottom current speed needed to suspend and transport coarse material on the shallow lagoon on the western periphery of Long Island. In particular, we need currents between 0.5 and 2 m/s (two orders of magnitude larger than ambient conditions) to generate coarse sediment transport.

4. Discussion

4.1. Event Attribution

4.1.1. Establishing a Modern Analog: Hurricane Joaquin 2015

We can gain a first order understanding of the sensitivity of our Long Island sediment proxy to different types of storm events by identifying which modern storms (1850 CE-present) left behind coarse deposits in the blue hole. This can be challenging given the high number of storms that have passed over The Bahamas in the past 169 years and the age uncertainties associated with each event layer. We cored LIBH less than a year after the island was impacted by a Category 4 hurricane, Hurricane Joaquin in 2015. This storm provides us with an excellent modern analog and gives us an idea of what wave conditions are sufficient for leaving an event deposit in LIBH.

Hurricane Joaquin formed as a tropical low in the eastern Atlantic Ocean on September 19, 2015. Joaquin moved southwest toward The Bahamas, strengthening to Category 4 strength on October 1st. A strong mid- to upper-level trough over the eastern US deepened on October 2nd causing Hurricane Joaquin to slow down and make a clockwise turn to the east of Long Island. It remained within 100 km of Long Island at Category 4 strength with sustained winds up to 62 m/s for an entire day. However, during this time, Hurricane Joaquin underwent an eyewall replacement cycle which resulted in an ill-defined eye in satellite imagery of Hurricane Joaquin as it passed Long Island on October 2nd. The storm caused severe flooding and damage to homes, vegetation, and local fishing vessels on Long Island. Indeed, two thirds of the island remained flooded with 1–2 m of water days after the storm (Berg, 2016).

Our cores from LIBH captured a large event bed starting 2 cm down in the core. This event bed (Event 1, Figure 5), unlike many others in the core, extends over 20 cm in thickness. Event bed thickness may be connected to storm duration. A longer lasting storm would transport more coarse-grained sediment into a basin assuming a plentiful supply of that sediment. The thickness of the uppermost event bed suggests it was likely deposited by a slower moving storm, like Hurricane Joaquin. Our age model dates this event bed to between 2011 and 2016 CE (median age: 2014). Since 2011 and prior to our initial 2016 coring, three hurricanes passed within 75 km of Long Island: Hurricane Joaquin in 2015, Hurricane Sandy in 2012, and Hurricane Irene in 2011 (Figures 5 and S9, Table S4). Satellite imagery indicates that the eyewall of Joaquin rested over LIBH for approximately 10 h. Both Sandy and Irene passed close to the island and at a faster translational velocity. Neither of their eyewalls rested over LIBH for a long time interval and both were significantly weaker than Joaquin (Avila & Cangialosi, 2011; Berg, 2016; Blake, Kimberlain et al., 2013). We cannot completely rule out that Hurricanes Sandy or Irene contributed to this unusually large event
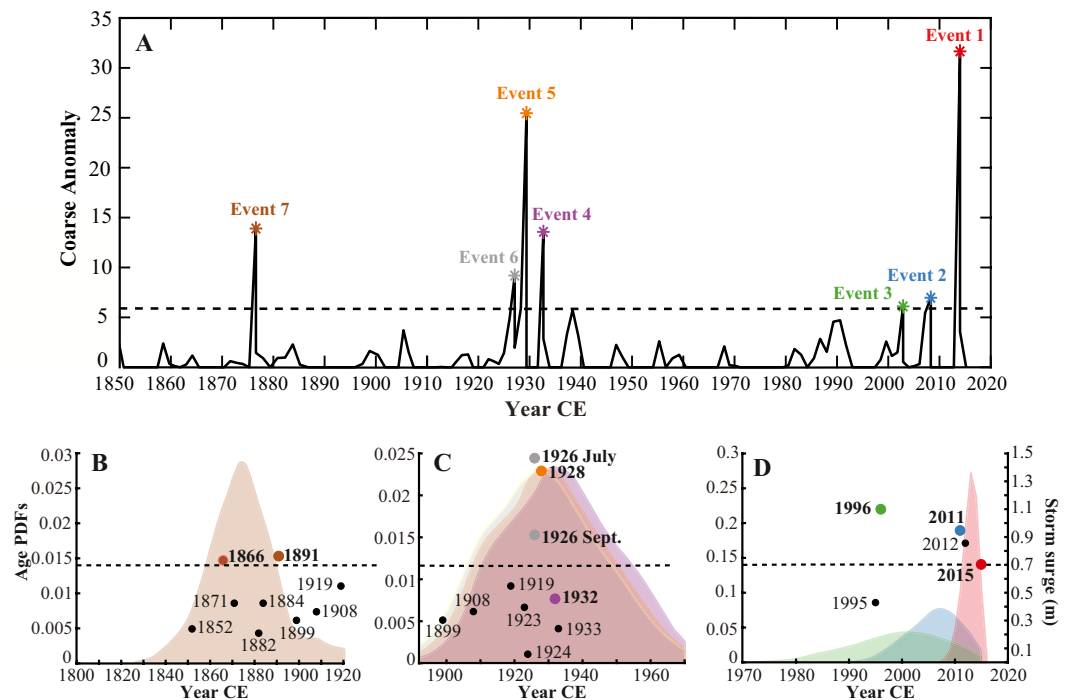
Figure 5. Coarse anomaly data for the modern interval (1850–2016) from LIBH2 (a). The dashed black line is the event bed threshold of 5.90%. Starred peaks indicate identified event layers. 95% age probability distributions for Event 7 (b), Events 4–6 (c), and Events 1–3 (d) shown in panel (a) Circles on panels (b)–(d) indicate the timing of observed storms passing with 100 km of LIBH plotted as a function of their levels of SLOSH simulated storm surge. The colored dots indicated the observational storms to which we attributed each event bed shown in panel (a) The dashed black lines in panels (b)–(d) denotes 0.7 m of surge simulated for our modern analog, Joaquin 2015. LIBH, Long Island Blue Hole.

bed. Indeed, the event bed does feature a secondary peak in grain size near the bottom of the deposit (Figure S10). However, given that the subsequent event bed occurs in such close proximity (only 5 cm down-core) to this larger more surficial coarse deposit, we attribute the first event bed to Hurricane Joaquin and the second event bed to one of these faster moving and less intense hurricanes (See Section 4.1.2).

A recent study (Sahoo et al., 2019) investigated the surge and wave dynamics on Long Island (and other Bahamian islands) during the passage of Hurricane Joaquin using the coupled ADCIRC-SWAN model (Dietrich, Westerink, et al., 2011, Dietrich, Zijlema, et al., 2011). They simulated wave heights (3–4 m), storm tides (0.5–1 m), and current speeds (~2 m/s) on the west coast of Long Island during the storm. The tidal range on Long Island is ~ 1 m (NOAA tide gauge station ID: TEC4633). We simulated ~0.7 m of storm surge on Long Island for Joaquin using SLOSH, a lower resolution and more simplified hydrodynamic model (Jelesnianski et al., 1992). SLOSH can only simulate the most idealized wind structures unlike more sophisticated models like ADCIRC-SWAN. Thus, it is likely less appropriate for storms like Hurricane Joaquin which underwent an eyewall replacement cycle as it made its closest passage to LIBH. Therefore, we should consider further storm surge results from SLOSH presented here as more conservative estimates of surge. In attributing the other modern deposits, we will use Hurricane Joaquin as modern analog. Thus, we know that storms passing to the east of the island that generate at least 0.7 m of storm surge may also have resulted in coarse-grained deposition in the blue hole.

4.1.2. Interpreting the Other Modern Deposits

Including Joaquin in 2015, 22 hurricanes passed within 100 km of the LIBH over the observational interval (1851-present). Yet, we only discovered seven event beds in the LIBH record that date within uncertainties to this same time interval (Figure 5). To attribute the other seven deposits, we used the criteria established using our modern analog (Hurricane Joaquin), historical observations, as well as storm surge estimates simulated using the SLOSH model (Jelesnianski et al., 1992). In general, storms passing proximal to and

east of Long Island created larger storm surge at LIBH (Figures 5 and S9). This is predominantly due to the L-shaped geometry of the northwest side of the island. When storms are passing to the north or east of the site, the counterclockwise rotational winds of the hurricane are in the same direction as waves piling water onshore. The opposite is true for storms moving to the south and west of the island. Indeed, our empirical data from the passage of Hurricane Irma in 2017 to the south of Long Island suggest that water was drained from the lagoon during this storm instead of piled up (Figure 4c). Storm surge estimates from SLOSH for historical storms ranged from 0.06 to 1.46 m at LIBH (Figure 5).

The second (2) and third (3) historical coarse-grained deposits follow shortly after the first event bed (attributed to Joaquin) and each extends less than 3 cm in thickness (Figure S10). Event 2 occurs between 28–30 cm in LIBH and dates between 1996 and 2015 CE (median age: 2008). Event 3 occurs between 35–36 cm in LIBH and dates between 1982 and 2014 CE (median age: 2003). Assuming that the first deposit is Hurricane Joaquin in 2015, there are only four storms that could have created these layers: Hurricane Sandy in 2012, Hurricane Irene in 2011, Hurricane Lili in 1996, and Hurricane Erin in 1995 (Figure 5d and Table S4). It is unlikely that Hurricane Erin generated either of these two event beds given its lower intensity (Category 1 with max sustained winds at 36 m/s). Despite its passage on the eastern side of the island (Figure S9), it only created ∼0.4 m of storm surge in SLOSH at the LIBH site (Table S4).

Hurricanes Lili, Irene, and Sandy all had much greater SLOSH-simulated storm surges of 1.1 m (20 min), 0.94 m (60 min), and 0.85 m (40 min), respectively (Figure 5d and Table S4). Both Hurricane Sandy and Hurricane Irene passed very close to Long Island (<25 km). Hurricane Sandy passed on the west side of the island at Category 2 strength (winds speeds up to 46 m/s). Disrupted by its passage over Cuba, Sandy was weakening and had lost most of its eye structure as it passed Long Island (Blake et al., 2013). Hurricane Irene, on the other hand, was more organized as it passed on the east side of Long Island transitioning from Category 3 to Category 2 strength with sustained wind speeds greater than 49 m/s (Avila & Cangialosi, 2011; Figure S9). Hurricane Lili in 1996 passed about 75 km to the north of Long Island with max sustained winds at 46 m/s (Category 2 strength). Lili was strengthening as it traveled north and east through The Bahamas such that its front right quadrant impacted the west coast of Long Island (Figure S9). In the Northern Hemisphere, the front right quadrant of a hurricane has both the rotational winds and movement of the storm in the same direction combining to create greater wind speeds and potentially greater storm surge. Although Lili passed further away from LIBH than either Hurricane Sandy or Irene, its radius of maximum winds was estimated between 55-75 km at the time of closest passage placing the eye wall of Lili directly over the blue hole (Lawrence, 1996). Indeed, we simulated approximately 1.1 m of surge during Hurricane Lili despite its lower Category 2 intensity (Figure 5d and Table S4).

We cannot determine for certain which of these three storms (i.e., Sandy 2012; Irene 2011; Lili 1996) left Event beds 2 and 3 in the LIBH sediment cores. We think it is more likely that Hurricane Irene in 2011 and Hurricane Lili in 1996 created these coarse beds (Table S4), given that both storms had stronger winds oriented onshore and generated more storm surge.

The next three event beds (#4–6) are grouped together starting at 96 cm in LIBH2. Each of these event beds is approximately 3 cm away from the next one suggesting that they occurred a few years apart (Figure 5c). Event beds 4, 5, and 6 date between 1903–1966 CE (median age: 1933), 1900–1963 CE (median age: 1929), and 1898–1962 CE (median age: 1927), respectively. Seven hurricanes passed within 100 km of Long Island from 1923-1933 CE (Table S4). Given the high number of storms that hit Long Island in rapid succession over this time period, we expect that this cluster of event beds corresponds to some subset of those seven storms.

Of the seven storms, only four were intense hurricanes (≥Category 3) passing within 75 km of the blue hole (Figure S9). On November 10, 1932, a Category 3 hurricane passed across Long Island just south of the blue hole with max sustained winds at 57 m/s. Just four years later on September 16, 1928, a Category 4 hurricane passed on the east side of the island with wind speeds at 69 m/s (coast.noaa.gov/hurricanes, 2020). Then in 1926, two intense hurricanes passed Long Island in July and September. The July Category 4 hurricane passed to the east of the island (sustained wind: 59–62 m/s) causing massive destruction. Both the light station at North End and Simms were blown away and 25 houses in Clarence Town were destroyed (Neely, 2006). In September, another Category 4 hurricane (sustained winds: 64 m/s) passed Long Island

on the western side (coast.noaa.gov/hurricanes, 2020). We attribute Event beds 4–6 to these four intense storms. Given our high sedimentation rate of ~1 cm/yr, we cannot determine which one of the intense 1926 hurricanes created Event bed 6. It is likely that both storms contributed to the event bed (Table S4). In general, storms passing on the eastern side on Long Island generated the largest storm surge estimates in SLOSH (1.37 m for the 1928 storm and 1.46 m for the July 1926 storm). The 1932 storm and September 1926 storm generated between 0.5 to 1 m less storm surge in SLOSH (Table S4).

The three other storms passed Long Island from 1923 to 1933 CE at much lower intensity (coast.noaa.gov/hurricanes, 2020). These storms, occurring in July 1933, November 1924, and September 1923, generated SLOSH storm surge estimates under 0.4 m at LIBH, and all three passed Long Island at Category 1 strength or lower (Figures 5 and S9). It is unlikely that these storms created Event beds 4 through 6 over the more intense and proximal storms in 1932, 1928, and 1926 which generated much larger storm surge at the blue hole (Figure 5).

Event bed 7 occurs between 148 and 168 cm (Figure 5b). Event bed 7 is another unusually thick layer stretching over 20 cm of sediment. Unfortunately, there is large age uncertainty for Event bed 7, which dates between 1848 and 1916 CE (median age: 1877). From 1850 to 1916 CE, seven more hurricanes track within 100 km of Long Island. In 1884, 1882, and 1852, Category 1 hurricanes tracked near Long Island. It is unlikely that any of these less intense storms created large enough wave energy to leave a deposit at LIBH. We simulated less than 0.5 m of storm surge at Long Island for each of these storms (Table S4, Figure S9).

There were four other storms that occurred from 1851 to 1916 CE: two Category 2 storms in 1891 and 1871, a Category 3 storm in 1899, and a Category 4 storm in 1866 (Table S4). Of these four storms, only two of them (1891 and 1866) passed within 75 km of Long Island (Figure S9). The 1899 Category 3 storm passed about 85 km to the southwest of LIBH. Its intensity, orientation and distance relative to the blue hole are all similar to Hurricane Matthew in 2016 (Figure S6). Surface sediments we collected from LIBH after Hurricane Matthew show no sign of coarse grains. Thus, it is unlikely that a storm of similar character (the 1899 hurricane) would leave Event bed 7 in LIBH2. The 1871 Category 2 storm passed east of Long Island approximately 85 km away and generated less than 0.5 m of surge in SLOSH. Given that both the 1891 and 1866 hurricanes generated roughly double this amount of surge in SLOSH (~0.8 m), it is more likely that one of these two storms generated Event bed 7.

Given the large age uncertainty associated with Event bed 7 and similar surge values simulated for both the 1891 and 1866 hurricanes (Figure 5), we cannot confidently determine which storm generated Event bed 7. We think it is more likely that the Category 4 1866 storm is the historical culprit for the seventh event bed. This storm passed within 75 km of LIBH on the western side of the island with sustained winds at 62 m/s (Figure S9). Written accounts of the storm suggest that Long Island was totally devastated with almost every building swept to the ground. Residents of the island suffered from starvation post storm and all of the cotton plantations were completely destroyed (Neely, 2006). However, we cannot rule out the 1891 hurricane as a potential candidate.

From our assessment of the observational storms, the LIBH record is capturing storms based not only on their intensity and proximity to the site but also on their orientation with respect to the island. LIBH captures all Category 2 and above storms passing to the east or north of Long Island within a 75 km radius of the site (Figure S9). This includes storms like Hurricane Joaquin 2015, Hurricane Irene 2011, and the 1928 and July 1926 Category 4 storms (Table S4). We also found that only the most intense hurricanes passing to the west of Long Island generated enough surge to leave a deposit (strong Category 3 (max sustained winds >55 m/s), 1932 storm; Category 4, the September 1926 storm and the 1866 Great Bahamas hurricane). In general, storms passing to the south or west of Long Island generated offshore directed winds which drew water off the carbonate lagoon on the west side of Long Island. The lower storm surge simulated during these storms (i.e., 1908 and 1899 storms) illustrate this phenomenon. Thus, we suggest that only the most intense of these western-passing storms (Category 4 and 5) could generate bottom currents strong enough to suspend and transport coarse material on the western Long Island lagoon.
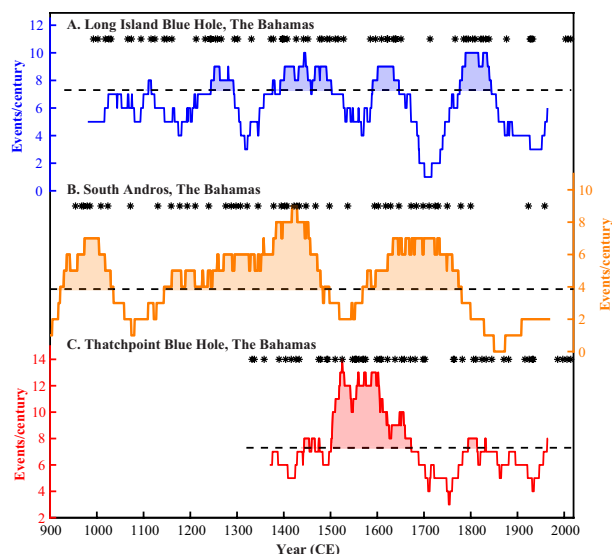
Figure 6. 100-year moving window event frequency for Bahamas reconstructions: (a) Long Blue Hole with 4 active intervals highlighted in blue, (b) South Andros stacked record (Wallace et al., 2019, Winkler et al, in review) with three active intervals highlighted in orange, and (c) Thatchpoint Blue Hole (Winkler et al., 2020; red) with one active interval highlighted in red. The active interval cutoff thresholds for each record are indicated by the dashed black lines. The timing of each event in the records is denoted by the black stars above each panel.

4.2. Caribbean Site Comparison

The resolution (near-annual) and length (1,050 years) of the LIBH core make it a good record to compare with the reconstruction from South Andros Island in The Bahamas (Wallace et al., 2019). Both records capture close-passing intense storms at near-annual resolution. In addition, both islands are in very close proximity; South Andros is situated approximately 260 km to the west of Long Island (Figure S6). We expected that during active intervals when more storms were traveling past South Andros Island, Long Island would also see more activity. Instead, the resulting patterns did not reflect our initial expectations (Figure 6). During the first (920–1035 CE) and last (1600–1780 CE) active intervals on South Andros, there is no concurrent increase in activity on Long Island (Figure 6). It is only for the second active interval on Andros Island that we observe any overlap with both islands observing increased hurricane strikes from 1350 to 1450 CE. Similarly, Long Island is active from 1590 to 1650 CE and 1775 to 1845 CE, periods of time when South Andros was experiencing relative quiescence. This carries on into the observational interval (1850-present). LIBH archived seven event deposits while the South Andros cores archived only two (Figure 6).

Perhaps even more puzzling is the difference we see between the Long Island, the South Andros records, and a new record of hurricane strikes over the past 700 years from Thatchpoint Blue Hole on Abaco Island, The Bahamas (Winkler et al., 2020). Abaco Island is approximately 400 km north-northwest of Long Island and ~275 km northeast of South Andros Island (Figure S6). The Thatchpoint record indicates elevated hurricane activity from 1500 to 1670 CE (Figure 6). During the peak of this activity on Abaco (the sixteenth century), both Long Island and South Andros show lower activity. They also both see an increase in activity during the early seventeenth century as activity at Thatchpoint is dying down. This increase in activity is short-lived for Long Island which experiences only one hurricane strike from 1651 to 1767 CE. South Andros, however, remains active throughout most of seventeenth and eighteenth centuries.

These differences between the three records raise questions about whether we should expect islands in the Caribbean spaced relatively close together (100s of kilometers) to observe similar patterns in intense hurricane activity on multi-decadal to centennial timescales. The tropical Atlantic (including The Bahamas) generally features climate conditions favorable for hurricane growth and survival (i.e., warm sea surface temperatures (SSTs), Emanuel, 2008; low vertical wind shear (VWS), Elsberry & Jeffries, 1996; Wong & Chan, 2004). Thus, storms are consistently traveling through the Caribbean. Given that the widespread climate conditions are favorable for hurricane survival, the direction these hurricanes track is likely dictated more by randomness of local conditions (i.e., steering winds, SSTs, topography), than by whole Atlantic or whole Caribbean climate conditions. Winkler et al. (2020) calculated 50-km grid track density of Category 2 and above hurricanes in the Atlantic over the observational interval (1850-present) and found spatial heterogeneity in track density in The Bahamas (Figure 1 in Winkler et al., 2020). In particular, their results indicate a gradient from lower activity over much of the Greater Antilles (e.g., Cuba, Haiti, Dominican Republic) to higher activity over the northern Bahamas. This is likely a result of a shadow effect created by storms losing intensity as they pass over the large island land masses of the Greater Antilles. South Andros falls within this shadow effect created by Cuba and shows notably less activity than Abaco Island. This suggests that at least over the last 169 years there has been localized differences in hurricane strike frequency in The Bahamas.

Assuming that hurricane tracks through The Bahamas contained similar variability in the past millennium as they do today, we need to combine many different sites in The Bahamas to capture changes in Bahamian hurricane climatology over the past millennium. The importance of stochasticity, geography, and regional climate/weather conditions almost certainly comes into play for determining if a storm of sufficient
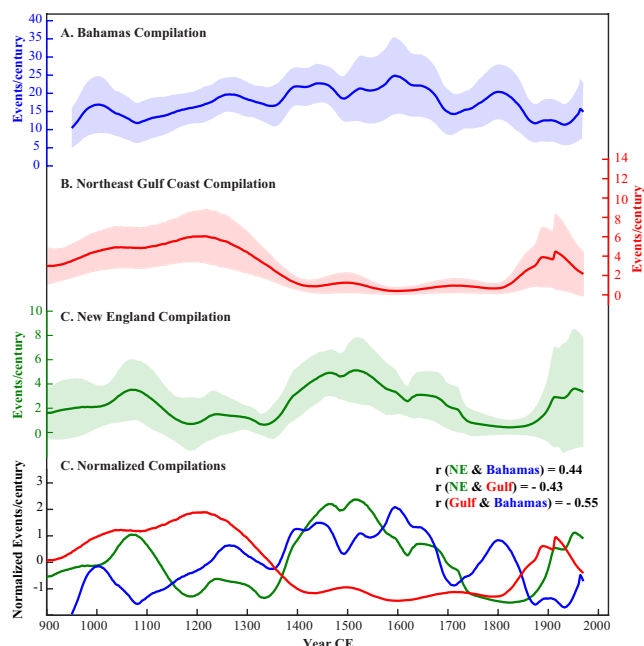
Figure 7. Compilations of paleohurricane records from (a) The Bahamas (blue) including all the records shown in Figure 6, (b) the Northeast Gulf Coast for intense events (red) including records from Mullet Pond, FL (Lane et al., 2011), Spring Creek Pond (Brandon et al., 2013), and Basin Bayou (Rodysill et al., 2020) and (c) New England (green) including records from Salt Pond, MA (Donnelly et al., 2015) and Mattapoisett Marsh (Boldt et al., 2010). The shaded confidence intervals are calculated from the spread in each of the contributing records. All three compilations shown were smoothed with a 100-year moving window. The original compilations (without the filter) are shown in Figure S12–S13. (d) All three regional compilations (panels (a)–(c)) normalized. Pearson correlation coefficients calculated for each combination of compilations are shown.

intensity will pass on one side of an island or another, or even whether it will pass close to a particular site. The blue holes studied on South Andros (Wallace et al., 2019) and Abaco Island (Winkler et al., 2020) capture storms passing within a 50 km radius. Like LIBH, Thatchpoint Blue Hole on Abaco Island is located in a subtidal carbonate lagoon (Bight of Abaco), but it is bordered by carbonate tidal flats to the east. On South Andros, the blue holes are more sheltered than LIBH (i.e., located inside carbonate tidal flat systems on the island). Looking at the tracks of the 24 hurricanes that passed within 75 km of Long Island in the last 170 years, only one and five of them passed within 50 km of South Andros and Thatchpoint, respectively (Figure S6). Given the differences in storm populations captured by these three records from The Bahamas, we should not use a single one of these records to describe Caribbean (or Bahamas for that matter) hurricane climatology over the past millennium. All three records are capturing different subsets of storms in The Bahamas passing over their particular location.

However, these same issues do not apply for all paleohurricane sites. In particular, sites in the subtropics (e.g., U.S. Northeast coastline) may capture a more cohesive climate signal simply due to their geography. Storms impacting the U.S. Northeast, for example, are typically moving in the north to northwestward direction parallel to the coast (Kossin et al., 2010). Therefore, paleohurricane sites in this region (Boldt et al., 2010; Donnelly et al., 2001, 2015) are generally impacted by many of the same storms and the same side of those storms (top left quadrant). In addition, unlike the Caribbean, climate is not always favorable for hurricane growth and survival in the subtropics throughout the hurricane season. Thus, it may require a strong climate signal to generate large numbers of storms repeatedly striking along the U.S. East Coast at hurricane intensity. Indeed, paleohurricane records spaced hundreds of kilometers apart along the U.S. East Coast show coherent active intervals over the past millennium. In particular, records from New England (Boldt et al., 2010; Buynevich & Donnelly, 2006; Donnelly et al, 2001, 2015; van de Plassche et al., 2006) and North Carolina (Mallinson et al., 2011) indicate elevated numbers of hurricanes striking during the fifteenth and sixteenth centuries.

4.3. Basin-Wide Comparison

Having noted many of the differences between paleohurricane records from The Bahamas, we created a compilation of Bahamas blue hole reconstructions including Long Island, South Andros, and Abaco Island (Figure 7a). The methods for creating this compilation were adapted from previous work (Mann, Woodruff, et al., 2009) and are described in detail in the Supplemental Material. The compilation offers a more cohesive picture of region-wide hurricane activity than a single individual Bahamas record. It shows increased activity from 975 to 1025 CE, 1400 to 1650 CE, and 1775 to 1825 CE. In addition, the combined Bahamas records indicate less hurricane activity over the observational interval (1850-present).

It is useful to further contextualize this Bahamas regional compilation through comparison to compilations of other similarly resolved records from along the U.S. coastline (Figures 7b and 7c). We generated compilations for New England using two records from Massachusetts and for the Northeast Gulf Coast including records from Apalachee Bay (Brandon et al., 2013; Lane et al., 2011; Rodysill et al., 2020) and Choctawhatchee Bay (Rodysill et al., 2020) in northwest Florida. In our Northeast Gulf Coast compilation, we created a high threshold compilation including only intense events (Category 3 and above). Our synthesis of these different U.S. coastal compilations gives us information on potential century-scale shifts in the predominance of certain storm populations in the North Atlantic (Figure 7d).

From approximately 900 to 1100 CE, we document evidence for a basin-wide increase in storm activity. This period of increased activity across the three compilations corresponds closely with the first half of the Medieval Warm Period (MWP) (900–1300; Mann, Zhang, et al., 2009). One potential driver of this basin-wide elevated activity is warmer SSTs in the Atlantic Main Development Region (MDR) which promotes tropical cyclone formation and potential intensity (Goldenberg et al., 2001; Kossin & Vimont, 2007; Zhang & Delworth, 2006). A statistical reconstruction of tropical cyclone activity driven by proxies of past climate change (Mann, Woodruff, et al., 2009) also shows this medieval period of increased Atlantic hurricane activity from 900 to 1100 CE. In this model, the active period arises predominantly due to a combination of La Nina-like conditions and warmer SSTs in the Atlantic MDR.

After 1100 CE, the Bahamas compilation correlates with the New England compilation ($r = 0.44$) but is anti-correlated with the Northeast Gulf Coast compilation ($r = -0.55$; Figure 7d). Following the period of basin-wide increased activity from 900 to 1100 CE, there is continued increased activity along the Gulf Coast that gradually declines through the fourteenth century accompanied by less activity in The Bahamas and New England. Starting around 1400 CE, this pattern shifts. More storms make landfall in The Bahamas and New England from 1400 to 1650 CE coeval with fewer intense storms in the Gulf. After a brief decline in activity at the end of the seventeenth century, there continues to be elevated storm strikes throughout much of The Bahamas through ~1825 CE while the Gulf coast of Florida and New England are quiet.

Our compilations reproduce hurricane patterns previously archived in a variety of lower resolution paleo-hurricane records from the U.S. Gulf and East Coasts. In the Gulf of Mexico, sediment records from Hancock County, Mississippi (Bregy et al., 2018) and the Florida Keys (Ercolani et al., 2015) also indicate increased storm strikes from 1150 to 1350 CE followed by lower storm activity from 1400 CE to present. Along the U.S. East Coast, marsh records from New England (Buynevich & Donnelly, 2006; Donnelly et al., 2001; van de Plassche et al., 2006) and a record of barrier island breaching from the Outer Banks in North Carolina (Mallinson et al., 2011) document increased storm strikes from 1400 to 1650 CE. Documentary records of Spanish shipwrecks in the Caribbean also indicate elevated storminess during the 1550–1640s (Trouet et al., 2016). Overall, this suggests that while our compilations only include records from New England and northwest Florida, they broadly represent cohesive hurricane patterns reconstructed along large swaths of the U.S. Gulf Coast and East Coast.

The Bahamas compilation differs from the other U.S. coastline compilations in the late eighteenth and early nineteenth centuries. During this period, we see increased hurricanes passing through The Bahamas while the other sediment compilations are quiet. Caribbean shipwreck records and tree ring proxies from the Florida Keys (Trouet et al., 2016), on the other hand, reproduce the patterns observed in our Bahamas compilation. All of these records show a decrease in activity from 1650 to 1715 CE followed by increased storm activity in the late eighteenth century. It is possible that during the late eighteenth century we are seeing a shift to more storms that recurve out into the north Atlantic Ocean. Documentary records from Bermuda (Tucker, 1982) and the Lesser Antilles (Chenoweth & Divine, 2008) support this hypothesis indicating increased storm landfalls observed from 1780 to 1840 CE.

An alternate explanation, first proposed in Donnelly et al. (2015), is that there were more storms traveling along U.S. East Coast during the late eighteenth and early nineteenth centuries, but they met with local unfavorable environmental conditions and were not high enough intensity to leave coarse event beds in coastal basins like Salt Pond (Donnelly et al., 2015) or Mattapoisett Marsh (Boldt et al., 2010). There is also documentary evidence for increased storms in the Southeast U.S. and Northeast U.S. from 1800 to 1900 CE. However, many of these storms were not very intense (≤Category 1) at landfall (Boose et al, 2001; Ludlum, 1963). Tree ring records of paleohurricane activity from Georgia (Grissino-Mayer et al., 2010; Miller et al., 2006) also capture multi-decadal periods of the increased storm strikes in the late eighteenth and early nineteenth centuries with five events recorded from 1773 to 1780 CE and 10 events recorded from 1800 to 1815 CE. The increased activity in The Bahamas ends around 1825 CE showing much fewer storms over the observational interval. At this point, we observe more storms making landfall in both northwest Florida and New England.

Our new Bahamas compilation supports previous work (Wallace et al., 2019) noting a shift over the last millennium from storms that impact the Gulf of Mexico (1150–1350 CE) to storms striking The Bahamas

and U.S. East Coast (1400–1650 CE). Two hypotheses could explain the shift in activity over the past millennium from increased activity in the Gulf of Mexico from 1150 to 1350 CE to activity along the U.S. East Coast from 1400 to 1650 CE. The first is the local environmental conditions hypothesis. This hypothesis suggests that from 1100 to 1350 CE there were more storms in the Atlantic basin in general, but there was a protective barrier of unfavorable environmental conditions (i.e., high VWS, low SSTs) along the U.S. East Coast extending down through the northern Bahamas. These unfavorable conditions caused hurricanes to weaken as they made their way up along the U.S. East Coast. This hypothesis is inspired by recent studies (Kossin, 2017; Ting et al., 2019) documenting a dipole pattern in environmental conditions (i.e., SSTs, VWS) between U.S. East Coast and Atlantic MDR over the past 50 years. The activity in our new compilation of Bahamas reconstructions presented here can still be at least partially explained by the environmental conditions hypothesis. We see decreased hurricane activity in both The Bahamas and U.S. East Coast when the Gulf Coast is active between 1100 and 1250 CE. Local unfavorable VWS conditions along the U.S. East Coast extending into The Bahamas, much like the pattern observed in Kossin (2017), coeval with basin-wide elevated activity could contribute to the decreased activity we observe in The Bahamas and along the U.S. East Coast.

Similarly, the subsequent opposite pattern of activity (i.e., increased activity in New England/The Bahamas with lower activity in the Gulf) extending from ∼1400–1650 CE can also be explained with the local environmental conditions hypothesis. Simulations of environmental conditions in the Atlantic under anthropogenic warming indicate patterns of increased VWS conditions in the Gulf of Mexico but not along U.S. East Coast (Ting et al., 2019). This anthropogenic VWS pattern is attributed to Hadley cell expansion (Kang & Lu, 2012; Lu et al., 2007) and a northward shift in the mid-latitude jet (Barnes & Polvani, 2013). The presence of a similar VWS pattern from 1400 to 1650 CE could explain the lack of intense storms making landfall near northwest Florida over this time span.

However, the local environmental conditions hypothesis is not the only possible explanation for the differences we observe between the U.S. East Coast and Gulf of Mexico records. A second hypothesis relies on the idea that there is climate driven geographic variability in hurricane tracks over the past millennium (Baldini et al., 2016; Elsner, 2003; Elsner et al., 2000; Liu & Fearn, 1993, 2000; Scott et al., 2003; Wallace et al., 2019; Xie et al., 2005). In particular, there might have been a shift from more straight-moving storms that impact the Caribbean Sea/Gulf of Mexico (Cluster 2 and 4, Kossin et al., 2010) from 1150 to 1250 CE to more recurving storms impacting The Bahamas and U.S. East Coast (Clusters 1 and 3, Kossin et al., 2010) from 1400 to 1650 CE.

While it is still uncertain exactly what climate conditions might produce these centennial-scale shifts in storm tracks, recent research suggests that shifts in the strength and position of subtropical ridges in the North Atlantic can impact hurricane tracks. In particular, the North Atlantic Subtropical High (NASH) has been shown to have a profound impact of steering currents in the North Atlantic (Elsner, 2003; Kossin et al., 2010; McCloskey et al., 2013; Ortegren & Maxwell, 2014). The NASH is a semi-permanent high pressure system located near Bermuda during the boreal summer (Davis et al., 1997; Zishka & Smith, 1980). When the NASH is strong and displaced toward the southwest, more hurricanes are straight-moving passing through the Caribbean Sea and Gulf of Mexico. The opposite is true when the NASH is weakened or displaced to the northeast (Elsner, 2003; Elsner & Kocher, 2000; Kossin et al., 2010; McCloskey et al., 2013; Ortegren & Maxwell, 2014; Scott et al., 2003). A high resolution reconstruction of the NASH is needed to further investigate its contribution (if any) to the centennial scale shifts in hurricane tracks we observe across our paleohurricane reconstructions.

Both of these hypotheses ignore the role of storms forming in the Gulf of Mexico and far western Caribbean. The increase in Gulf Coast landfalling storms captured in our Northeast Gulf Coast compilation from 1100 to 1250 CE could reflect a century-scale change in Gulf of Mexico/western Caribbean storm genesis. Unfortunately, the controlling mechanisms for genesis in these regions of the Atlantic are understudied. Previous work has shown a connection between Gulf of Mexico-forming storms and the Madden-Julian Oscillation (MJO) (Kossin et al., 2010; Maloney & Hartmann, 2000). The MJO is a 30 to 60-day fluctuation in tropical circulation that moves eastward along the equator initiating alternating westerly and easterly wind anomalies over the eastern Pacific (Zhang et al., 2020). During westerly MJO periods, there are enhanced cyclonic anomalies over the western Caribbean and Gulf of Mexico which can promote increased tropical cyclone

genesis in these regions (Kossin et al., 2010; Maloney & Hartmann, 2000). The fundamental physics behind the MJO and its global influences are still under debate in the scientific community (Zhang et al., 2020) and thus, more work is needed to establish a connection between MJO and Gulf hurricanes, especially on long-timescales.

5. Conclusions

This work presents a new near-annually resolved reconstruction of intense hurricane activity over the past 1,050 years from a blue hole on the northwest coast of Long Island in The Bahamas. Unlike other paleohurricane sites from the Atlantic, many intense storms made landfall on Long Island during the observational record (1850-present). The sediment cores from LIBH capture seven event beds dating to historic hurricanes. Attributing these event beds to modern storms highlights that using simple thresholds based on the intensity of each storm and its proximity to a site does not capture the wide variety of hydrodynamics that could create event deposition. Using storm surge estimates from SLOSH, we find that the location of our site relative to the coastline and coastline geometry play a very important role in determining whether or not a storm left a deposit. In particular, the L-shaped geometry of the northwest side of Long Island promoted larger storm surge for storms passing to the north or east. Only the most intense storms (Category 4 and 5) passing to the south or west generated enough surge to leave a deposit in LIBH.

Data collected from after Hurricane Matthew in 2016 and Hurricane Irma in 2017 confirm these conclusions. Both storms passed on the western side of Long Island further than 75 km away from LIBH at high intensity and neither of them left a coarse deposit at the bottom of LIBH. Indeed, bottom current speed and direction data collected near the blue hole in September 2017 suggest that the more distal passage of Irma on the western side of the island drained the lagoon of water during the peak of the storm. This highlights that storm deposition in blue hole environments is affected not only by the characteristics of the storms themselves (i.e., intensity) but also by the variability in the local hydrodynamic response related to storm passage, island geometry, and the characteristics of the depositional environments. More work is needed modeling how different properties of storms (i.e., translational velocity, track orientation, wind speeds) affects the hydrodynamics and sediment transport in different depositional environments (i.e., carbonate lagoon vs. tidal flat).

Long Island has experienced four multi-decadal periods of elevated intense hurricane activity over the past millennium (1245–1290 CE, 1395–1500 CE, 1590–1650 CE, and 1775–1845 CE). These active periods contrast with event frequency patterns reconstructed at two neighboring islands (Abaco Island, Winkler et al., 2020 and South Andros Island, Wallace et al., 2019). We argue that these three islands while relatively close together (<500 km apart) have captured largely different populations of hurricanes. This is confirmed looking at the storms that passed over Long Island in the last 169 years; only a few of these storms went on to hit Abaco or South Andros Island. We argue that the signals reconstructed in each individual record from The Bahamas are heavily influenced by randomness, geography, and site sensitivity. This makes it difficult to make useful comparisons between different records or to use any one record to reconstruct regional hurricane climate. In order to capture regional hurricane patterns over time, we need to start combining proxies from neighboring sites in The Bahamas together into a regional composite.

Thus, we present the first compilation of Bahamian paleohurricane reconstructions for the past millennium (900–2016 CE). The compilations better capture the regional hurricane record by compositing each individual island's storm history. The Bahamas compilation documents elevated storm activity from 975–1025 CE, 1400–1650 CE, and 1775–1825 CE. Much like other paleohurricane reconstructions from the Atlantic basin, this compilation shows lower storm activity over the past 150 years. This further confirms that the hurricane activity we've observed in the Bahamas recently is on the lower end of what's occurred in the Atlantic over the past 1,000 years.

Compilations from the U.S. coastline (both New England and the Northeast Gulf of Mexico) confirm the increased hurricane activity reconstructed from 900 to 1100 CE suggesting that the North Atlantic basin was active over this time period. An independent statistical simulation of tropical cyclones over the past millennium (Mann, Woodruff, et al., 2009) also shows this increased activity during this medieval period, predominantly due to warmer SSTs in the Atlantic MDR and more La Nina-like conditions in the Pacific.

From 1100 CE to present, we see a shift from elevated basin-wide activity to shifts in the predominance of certain storm populations in the Atlantic. The Bahamas compilation matches with the New England compilation and contrasts with the Gulf Coast compilation. We suggest that these contrasting patterns of hurricane activity reflect a shift over the past millennium from a more straight-moving populations of storm tracks that impact the Gulf Coast (1100–1250 CE) to more recurving storm tracks hitting The Bahamas and U.S. East Coast (1400–1650 CE) tied to changes in the NASH (e.g., Kossin et al., 2010; Liu & Fearn, 1993; McCloskey et al., 2013) and/or a shift from unfavorable local environmental conditions along U.S. East Coast and Bahamas (e.g., Kossin, 2017; Ting et al., 2019) from 1100 to 1250 CE to unfavorable conditions along the Gulf Coast from 1400 to 1650 CE.

Data Availability Statement

The data are available on the National Climatic Data Center (https://www.ncdc.noaa.gov/paleo/study/32134) and WHOI Coastal Systems Group (https://web.whoi.edu/coastal-group/data/) websites.

References

Appleby, P. G. (2001). Chronostratigraphic Techniques in Recent Sediments. In W. M. Last, & J. P. Smol, (Eds.), *Tracking environmental change using lake sediments: Volume 2: Physical and geochemical methods* (pp. 171–202). New York, NY: Kluwer Academic Publishers.

Appleby, P. G., & Oldfield, F. (1978). The Calculation of Lead-210 dates assuming a constant rate of supply of unsupported 210-Pb to the sediment. *Catena*, *5*, 1–8.

Avila, L. A., & Cangialosi, J. P. (2011). *Tropical cyclone report hurricane Irene AL092011*.

Baldini, L. M., Baldini, J. U. L., McElwaine, J. N., Frappier, A. B., Asmerom, Y., Liu, K., et al. (2016). Persistent northward North Atlantic tropical cyclone track migration over the past five centuries. *Scientific Reports*, *6*(1). https://doi.org/10.1038/srep37522

Barnes, E., & Polvani, L. (2013). Response of the midlatitude jets, and of their variability, to increased greenhouse gases in the CMIP5 models. *Journal of Climate*, *26*(2007), 7117–7135. https://doi.org/10.1175/JCLI-D-12-00536.1

Berg, R. J. (2016). Hurricane Joaquin (AL112015). In *National hurricane center tropical cyclone report (issue January)*.

Bhatia, K., Vecchi, G., Murakami, H., Underwood, S., & Kossin, J. (2018). Projected response of tropical cyclone intensity and intensification in a global climate model. *Journal of Climate*, *31*(20), 8281–8303. https://doi.org/10.1175/JCLI-D-17-0898.1

Blaauw, M., & Christen, J. A. (2011). Flexible paleoclimate age-depth models using an autoregressive gamma process. *Bayesian Analysis*, *6*(3), 457–474. https://doi.org/10.1214/11-BA618

Blake, E. S., Kimberlain, T. B., Berg, R. J., Cangialosi, J. P., & Beven, J. L. (2013). *Tropical cyclone report hurricane Sandy AL182012*.

Boldt, K. V., Lane, P., Woodruff, J. D., & Donnelly, J. P. (2010). Calibrating a sedimentary record of overwash from Southeastern New England using modeled historic hurricane surges. *Marine Geology*, *275*(1–4), 127–139. https://doi.org/10.1016/j.margeo.2010.05.002

Boose, E. R., Chamberlin, K. E., & Foster, D. R. (2001). Landscape and regional impacts of hurricanes in New England. *Ecological Monographs*, *71*(1), 27–48. https://doi.org/10.1890/0012-9615(2001)071[0027:LARIOH#x005D;2.0.CO;2

Brandon, C. M., Woodruff, J. D., Lane, D. P., & Donnelly, J. P. (2013). Tropical cyclone wind speed constraints from resultant storm surge deposition: A 2500-year reconstruction of hurricane activity from St. Marks, FL. *Geochemistry, Geophysics, Geosystems*, *14*(8), 2993–3008. https://doi.org/10.1002/ggge.20217

Bregy, J. C., Wallace, D. J., Minzoni, R. T., & Cruz, V. J. (2018). 2500-year paleotempestological record of intense storms for the northern Gulf of Mexico, United States. *Marine Geology*, *396*, 26–42. https://doi.org/10.1016/j.margeo.2017.09.009

Brown, A. L., Reinhardt, E. G., van Hengstum, P. J., & Pilarczyk, J. E. (2014). A coastal yucatan sinkhole records intense hurricane events. *Journal of Coastal Research*, *30*(2), 418–429. https://doi.org/10.2112/JCOASTRES-D-13-00069.1

Buynevich, I. V., & Donnelly, J. P. (2006). Geological signatures of barrier breaching and overwash, southern Massachusetts, USA. *Journal of Coastal Research*, *I*(39), 112–116.

Cangialosi, J. P., Latto, A. S., & Berg, R. (2018). Hurricane Irma (AL112017). In *National hurricane center tropical cyclone report (issue June)*.

Chenoweth, M., & Divine, D. (2008). A document-based 318-year record of tropical cyclones in the Lesser Antilles, 1690-2007. *Geochemistry, Geophysics, Geosystems*, *9*(8), 1–21. https://doi.org/10.1029/2008GC002066

Clark, J. S., & Patterson, W. A. I. (1984). Pollen, Pb-210, and opaque spherules: an integrated approach to dating and sedimentation in the intertidal environment. *Journal of Sedimentary Petrology*, *54*(4), 1251–1265.

Correll, D. S., & Correll, H. B. (1982). *Flora of the Bahama archipelago: Including the Turks and Caicos islands*. A. R. G. Verlag.

Craton, M. (1968). *A history of the Bahamas* (2nd ed.). Collins Clear-Type Press.

Craton, M., & Saunders, G. (1992). *Islanders in the stream: A history of the Bahamian people: Volume one: From aboriginal times to the end of slavery*. Athens, GA: University of Georgia Press.

Craton, M., & Saunders, G. (1998). *Islanders in the stream: A history of the Bahamian people: Volume two: From the ending of slavery to twenty-first century*. Athens, GA: University of Georgia Press.

Davis, R., Hayden, B., Gay, D., Phillips, W., & Jones, G. (1997). The North Atlantic subtropical anticyclone. *Journal of Climate*, *10*, 728–744.

Denommee, K. C., Bentley, S. J., & Droxler, A. W. (2014). Climatic controls on hurricane patterns: A 1200-y near-annual record from Lighthouse Reef, Belize. *Scientific Reports*, *4*. https://doi.org/10.1038/srep03876

Dietrich, J. C., Westerink, J. J., Kennedy, A. B., Smith, J. M., Jensen, R. E., Zijlema, M., et al. (2011). Hurricane Gustav (2008) waves and storm surge: Hindcast, synoptic analysis, and validation in Southern Louisiana. *Monthly Weather Review*, *139*, 2488–2522. https://doi.org/10.1175/2011MWR3611.1

Dietrich, J. C., Zijlema, M., Westerink, J. J., Holthuijsen, L. H., Dawson, C., Luettich, R. A., Jr., et al. (2011). Modeling hurricane waves and storm surge using integrally-coupled, scalable computations. *Coastal Engineering*, *58*, 45–65. https://doi.org/10.1016/j.coastaleng.2010.08.001

Donnelly, J. P., Bryant, S. S., Butler, J., Dowling, J., Fan, L., Hausmann, N., et al. (2001). 700 yr sedimentary record of intense hurricane landfalls in southern New England. The *Geological Society of America Bulletin*, *113*(6), 714–727.

Donnelly, J. P., Hawkes, A. D., Lane, P., Macdonald, D., Shuman, B. N., Toomey, M. R., et al. (2015). Climate forcing of unprecedented intense-hurricane activity in the last 2000 years. *Earth's Future*, *3*(2), 49–65. https://doi.org/10.1002/2014EF000274

Donnelly, J. P., & Woodruff, J. D. (2007). Intense hurricane activity over the past 5,000 years controlled by El Niño and the West African monsoon. *Nature*, *447*(7143), 465–468. https://doi.org/10.1038/nature05834

Elsberry, R. L., & Jeffries, R. A. (1996). Vertical Wind Shear Influences on Tropical Cyclone Formation and Intensification during TCM-92 and TCM-93. *Monthly Weather Review*, *124*, 1374–1387.

Elsner, J. B. (2003). Tracking hurricanes. *Bulletin of the American Meteorological Society*, *84*(3), 353–356. https://doi.org/10.1175/BAMS-84-3-353

Elsner, J. B., & Kocher, B. (2000). Global tropical cyclone activity: A link to the North Atlantic oscillation. *Journal of Geophysical Research*, *27*(1), 129–132. https://doi.org/10.1029/1999GL010893

Elsner, J. B., Liu, K., & Kocher, B. (2000). Spatial variations in major U.S. hurricane activity: Statistics and a physical mechanism. *Journal of Climate*, *13*, 2293–2305. https://doi.org/10.1175/1520-0442(2000)013<2293:SVIMUS>2.0.CO;2

Emanuel, K. (2008). The hurricane-climate connection. *Bulletin of the American Meteorological Society*, *89*(5), ES10–ES20. https://doi.org/10.1175/BAMS-89-5-Emanuel

Emanuel, K. A. (2013). Downscaling CMIP5 climate models shows increased tropical cyclone activity over the 21st century. *Proceedings of the National Academy of Sciences*, *110*(30), 12219–12224. https://doi.org/10.1073/pnas.1301293110

Eneas, W. J. G. (1998). *Agriculture in the Bahamas: Its historical development 1492-1992*. Media Publishing.

Ercolani, C., Muller, J., Collins, J., Savarese, M., & Squiccimara, L. (2015). Intense Southwest Florida hurricane landfalls over the past 1000 years. *Quaternary Science Reviews*, *126*. https://doi.org/10.1016/j.quascirev.2015.08.008

Goldenberg, S. B., Landsea, C. W., Mestas-Nuñez, A. M., & Gray, W. M. (2001). The Recent increase in Atlantic hurricane activity: Causes and implications. *Science*, *293*(5529), 474–479. https://doi.org/10.1126/science.1060040

Griffin, J. J., & Goldberg, E. D. (1975). The fluxes of elemental carbon in coastal marine sediments. *Limnology & Oceanography*, *20*(3), 456.

Grissino-Mayer, H. D., Miller, D. L., & Mora, C. I. (2010). Dendrotempestology and the isotopic record of tropical cyclones in tree rings of the southeastern United States. In M. Stoffel, M. Bollschweiler, D. R. Butler, & B. H. Luckman, Eds., *Tree rings and natural hazards: A state-of-the-art* (pp. 291–303). New York, NY: Springer. https://doi.org/10.1007/978-90-481-8736-2

Jelesnianski, C. P., Chen, J., & Shaffer, W. A. (1992). *SLOSH: Sea, Lake and Overland surges from hurricanes*.

Kang, S. M., & Lu, J. (2012). Expansion of the Hadley Cell under Global Warming: Winter versus Summer. *Journal of Climate*, *25*, 8387–8393. https://doi.org/10.1175/JCLI-D-12-00323.1

Kishore, N., Marques, D., Mahmud, A., Kiang, M., Rodriguez, I., Fuller, A., et al. (2018). Mortality in Puerto Rico after Hurricane Maria. *New England Journal of Medicine*, *379*(2), 162–170. https://doi.org/10.1056/NEJMsa1803972

Knapp, K., Kruk, M. C., Levinson, D. H., Diamond, H. J., & Neumann, C. J. (2010). The International Best Track Archive for Climate Stewardship (IBTrACS). *Bulletin of the American Meteorological Society*, *91*(3), 363–376. https://doi.org/10.1175/2009BAMS2755.1

Knutson, T., Camargo, S. J., Chan, J. C. L., Emanuel, K., Ho, C., Kossin, J. P., et al. (2019). Tropical cyclones and climate change assessment: Part I. Detection and attribution. *Bulletin of the American Meteorological Society*, *100*(10), 1987–2007. https://doi.org/10.1175/BAMS-D-18-0189.1

Korty, R. L., Emanuel, K. A., Huber, M., & Zamora, R. A. (2017). Tropical cyclones downscaled from simulations with very high carbon dioxide levels. *Journal of Climate*, *30*(2), 649–667. https://doi.org/10.1175/JCLI-D-16-0256.1

Kossin, J. P. (2017). Hurricane intensification along United States coast suppressed during active hurricane periods. *Nature*, *541*(7637), 390–393. https://doi.org/10.1038/nature20783

Kossin, J. P., Camargo, S. J., & Sitkowski, M. (2010). Climate modulation of North Atlantic hurricane tracks. *Journal of Climate*, *23*(11), 3057–3076. https://doi.org/10.1175/2010JCLI3497.1

Kossin, J. P., & Vimont, D. J. (2007). A more general framework for understanding atlantic hurricane variability and trends. *Bulletin of the American Meteorological Society*, *88*(11), 1767–1781. https://doi.org/10.1175/BAMS-88-11-1767

Lane, P., Donnelly, J. P., Woodruff, J. D., & Hawkes, A. D. (2011). A decadally-resolved paleohurricane record archived in the late Holocene sediments of a Florida sinkhole. *Marine Geology*, *287*(1–4), 14–30. https://doi.org/10.1016/j.margeo.2011.07.001

Lawrence, M. B. (1996). *Preliminary report* (pp. 14–27). Hurricane Lili.

Lin, N., Emanuel, K. A., Smith, J. A., & Vanmarcke, E. (2010). Risk assessment of hurricane storm surge for New York city. *Journal of Geophysical Research*, *115*(D18121), 1–11. https://doi.org/10.1029/2009JD013630

Lin, N., Lane, P., Emanuel, K. A., Sullivan, R. M., & Donnelly, J. P. (2014). Heightened hurricane surge risk in northwest Florida revealed from climatological-hydrodynamic modeling and paleorecord reconstruction. *Journal of Geophysical Research: Atmosphere*, *119*(14), 1–18. https://doi.org/10.1002/2014JD021584

Little, B. G., Buckley, D. K., Cant, R., Henry, P. W. T., Jefferiss, A., Mather, J. D., et al. (1977). *Land resources of the Bahamas: A summary*. Land Resources Division, Ministry of Overseas Development.

Liu, K., & Fearn, M. L. (1993). Lake-sediment record of late Holocene hurricane. *Geology*, *21*(September), 793–796. https://doi.org/10.1130/0091-7613(1993)021<0793

Liu, K., & Fearn, M. L. (2000). Reconstruction of prehistoric landfall frequencies of catastrophic hurricanes in northwestern Florida from lake sediment records. *Quaternary Research*, *54*(2), 238–245. https://doi.org/10.1006/qres.2000.2166

Lu, J., Vecchi, G. A., & Reichler, T. (2007). Expansion of the Hadley cell under global warming. *Geophysical Research Letters*, *34*, 2–6. https://doi.org/10.1029/2006GL028443

Ludlum, D. M. (1963). *Early American hurricanes, 1492-1870*. Boston, MA: American Meterological Society.

Mallinson, D. J., Smith, C. W., Mahan, S., Culver, S. J., & McDowell, K. (2011). Barrier island response to late Holocene climate events, North Carolina, USA. *Quaternary Research*, *76*(1), 46–57. https://doi.org/10.1016/j.yqres.2011.05.001

Maloney, E. D., & Hartmann, D. L. (2000). Modulation of hurricane activity in the Gulf of Mexico by the Madden-Julian oscillation. *Science*, *287*(5460), 2002–2004. https://doi.org/10.1126/science.287.5460.2002

Mann, M. E., Woodruff, J. D., Donnelly, J. P., & Zhang, Z. (2009). Atlantic hurricanes and climate over the past 1,500 years. *Nature*, *460*(7257), 880–883. https://doi.org/10.1038/nature08219

Mann, M. E., Zhang, Z., Rutherford, S., Bradley, R. S., Hughes, M. K., Shindell, D., et al. (2009). Global signatures and dynamical origins of the little ice age and medieval climate anomaly. *Science*, *326*(5957), 1256–1260. https://doi.org/10.1126/science.1177303

McCloskey, T., Bianchette, T., & Liu, K. (2013). Track patterns of landfalling and coastal tropical cyclones in the Atlantic basin, their relationship with the North Atlantic Oscillation (NAO), and the potential effect of global warming. *American Journal of Climate*, *2*, 12–22. https://doi.org/10.4236/ajcc.2013.23A002

McCloskey, T. A., & Liu, K. B. (2012). A 7000 year record of paleohurricane activity from a coastal wetland in Belize. *The Holocene*, *23*(2), 278–291. https://doi.org/10.1177/0959683612460782

Mendelsohn, R., & Emanuel, K., Chonabayashi, S., & Bakkensen, L. (2012). The impact of climate change on global tropical cyclone damage. *Nature Climate Change*, *2*, 205–209. https://doi.org/10.1038/nclimate1357

Miller, D. L., Mora, C. I., Grissino-Mayer, H. D., Mock, C. J., Uhle, M. E., & Sharp, Z. (2006). Tree-ring isotope records of tropical cyclone activity. *Proceedings of the National Academy of Sciences*, *103*(39), 14294–14297.

Miller, M. C., McCave, I. N., & Komar, P. D. (1977). Threshold of sediment motion under unidirectional currents. *Sedimentology*, *24*(4), 507–527. https://doi.org/10.1111/j.1365-3091.1977.tb00136.x

Mylroie, J. E., Carew, J. L., & Moore, A. I. (1995). *Blue holes: Definition and genesis. Carbonates and evaporites*. https://doi.org/10.1007/BF03175407

Neely, W. (2006). *The major hurricanes to affect the Bahamas*. AuthorHouse.

Neely, W. (2013). *The Great Bahamas hurricane of 1929*. iUniverse LLC.

Ortegren, J. T., & Maxwell, J. T. (2014). Spatiotemporal patterns of drought/tropical cyclone co-occurrence in the southeastern USA: Linkages to North Atlantic climate variability. *Geography Compass*, *8*, 540–559.

Pasch, R. J., Penny, A. B., & Berg, R. (2019). Hurricane Maria (AL152017). In *National hurricane center tropical cyclone report (issue February)*.

Pielke, R. a., Jr., Gratz, J., Landsea, C. W., Collins, D., Saunders, M. A., & Musulin, R. (2008). Normalized Hurricane Damage in the United States: 1900–2005. *Natural Hazards Review*, *9*(February), 29–42. https://doi.org/10.1061/(ASCE)1527-6988(2008)9:1(29)

Reimer, P. J., Brown, T. A., & Reimer, R. W. (2004). Discussion: Reporting and calibration of post-bomb 14C data. *Radiocarbon*, *46*(1), 1299–1304. https://doi.org/10.2458/azu_js_rc.46.4183

Rodysill, J., Donnelly, J. P., Sullivan, R. M., Lane, P. D., Toomey, M. R., Woodruff, J. D., et al. (2020). Historically unprecedented Northern Gulf of Mexico hurricane activity from 650 to 1250 CE. *Scientific Reports*, *10*, 1–17. https://doi.org/10.1038/s41598-020-75874-0

Sahoo, B., Jose, F., & Bhaskaran, P. K. (2019). Hydrodynamic response of Bahamas archipelago to storm surge and hurricane generated waves – A case study for Hurricane Joaquin. *Ocean Engineering*, *184*, 227–238.

Schmitt, D., Gischler, E., Anselmetti, F. S., & Vogel, H. (2020). Caribbean cyclone activity: An annually-resolved Common Era record. *Scientific Reports*, *10*, 1–17. https://doi.org/10.1038/s41598-020-68633-8

Scott, D. B., Collins, E. S., Gayes, P. T., & Wright, E. (2003). Records of prehistoric hurricanes on the South Carolina coast based on micropaleontological and sedimentological evidence, with comparison to other Atlantic Coast records. *The Geological Society of America Bulletin*, *115*(9), 1027–1039.

Sobel, A. H., Camargo, S. J., Hall, T. M., Lee, C. Y., Tippett, M. K., & Wing, A. A. (2016). Human influence on tropical cyclone intensity. *Science*, *353*(6296), 242–246. https://doi.org/10.1126/science.aaf6574

Ting, M., Kossin, J. P., Camargo, S. J., & Li, C. (2019). Past and future hurricane intensity change along the U. S. east coast. *Scientific Reports*, *9*(7795), 1–8. https://doi.org/10.1038/s41598-019-44252-w

Trouet, V., Harley, G. L., & Domínguez-Delmás, M. (2016). Shipwreck rates reveal Caribbean tropical cyclone response to past radiative forcing. *Proceedings of the National Academy of Sciences*, *113*(12). https://doi.org/10.1073/pnas.1519566113

Tucker, T. (1982). *Beware the hurricane!*. Washington, DC: Island Press.

Ulm, K. (1990). A simple method to calculate the confidence interval of a standardized mortality ratio (SMR). *American Journal of Epidemiology*, *131*(2), 373–375. https://doi.org/10.1093/oxfordjournals.aje.a115507

van de Plassche, O., Erkens, G., van Vliet, F., Brandsma, J., van der Borg, K., & de Jong, A. F. M. (2006). Salt-marsh erosion associated with hurricane landfall in southern New England in the fifteenth and seventeenth centuries. *Geology*, *34*(10), 829–832. https://doi.org/10.1130/G22598.1

van Hengstum, P. J., Donnelly, J. P., Fall, P. L., Toomey, M. R., Albury, N. A., & Kakuk, B. (2016). The intertropical convergence zone modulates intense hurricane strikes on the western North Atlantic margin. *Scientific Reports*, *6*(October 2015), 21728. https://doi.org/10.1038/srep21728

van Hengstum, P. J., Donnelly, J. P., Toomey, M. R., Albury, N. A., Lane, P., & Kakuk, B. (2014). Heightened hurricane activity on the Little Bahama Bank from 1350 to 1650 AD. *Continental Shelf Research*, *86*, 103–115. https://doi.org/10.1016/j.csr.2013.04.032

van Hengstum, P. J., Scott, D. B., Gröcke, D. R., & Charette, M. A. (2011). Sea level controls sedimentation and environments in coastal caves and sinkholes. *Marine Geology*, *286*(1–4), 35–50. https://doi.org/10.1016/j.margeo.2011.05.004

van Hengstum, P. J., Winkler, T. S., Tamalavage, A. E., Sullivan, R. M., Little, S. N., Macdonald, D., et al. (2020). Holocene sedimentation in a blue hole surrounded by carbonate tidal flats in The Bahamas: Autogenic versus allogenic processes. *Marine Geology*, *419*. https://doi.org/10.1016/j.margeo.2019.106051

Wallace, D. J., Woodruff, J. D., Anderson, J. B., & Donnelly, J. P. (2014). Palaeohurricane reconstructions from sedimentary archives along the Gulf of Mexico, Caribbean Sea and western North Atlantic Ocean margins. *Sedimentary Coastal Zones from High to Low Latitudes: Similarities and Differences*, *388*, 481–501. https://doi.org/10.1144/SP388.12

Wallace, E. J., Donnelly, J. P., van Hengstum, P. J., Wiman, C., Sullivan, R. M., Winkler, T. S., et al. (2019). Intense hurricane activity over the past 1500 years at South Andros Island, The Bahamas. *Paleoceanography and Paleoclimatology*, *34*(11), 1761–1783. https://doi.org/10.1029/2019PA003665

Walsh, K. J. E., Mcbride, J. L., Klotzbach, P. J., Balachandran, S., Camargo, S. J., Holland, G., et al. (2016). Tropical cyclones and climate change. *Wiley Interdisciplinary Reviews: Climate Change*, *7*(1). https://doi.org/10.1002/wcc.371

Winkler, T. S., Van Hengstum, P. J., Donnelly, J. P., Wallace, E. J., Sullivan, R. M., Macdonald, D., & Albury, N. A. (2020). Revising evidence of hurricane strikes on Abaco Island (The Bahamas) over the last 680 years. *Scientific Reports*, *10*. Retrieved from https://www.nature.com/articles/s41598-020-73132-x

Wong, M. L. M., & Chan, J. C. L. (2004). Tropical cyclone intensity in vertical wind shear. *Journal of the Atmospheric Sciences*, *61*, 1859–1876.

Woodruff, J. D., Irish, J. L., & Camargo, S. J. (2013). Coastal flooding by tropical cyclones and sea-level rise. *Nature*, *504*(7478). https://doi.org/10.1038/nature12855

Xie, L., Yan, T., Pietrafesa, L. J., Morrison, J. M., & Karl, T. (2005). Climatology and interannual variability of North Atlantic hurricane tracks. *Journal of Climate*, *18*(24), 5370–5381. https://doi.org/10.1175/JCLI3560.1

Zhang, C., Adames, F., Khouider, B., Wang, B., & Yang, D. (2020). Four theories of the Madden-Julian oscillation. *Reviews of Geophysics*, *58*(3), 1–55. https://doi.org/10.1029/2019RG000685

Zhang, L., Karnauskas, K. B., Donnelly, J. P., & Emanuel, K. (2017). Response of the North Pacific tropical cyclone climatology to global warming: Application of dynamical downscaling to CMIP5 models. *Journal of Climate*, *30*(4), 1233–1243. https://doi.org/10.1175/JCLI-D-16-0496.1

Zhang, R., & Delworth, T. L. (2006). Impact of Atlantic multidecadal oscillations on India/Sahel rainfall and Atlantic hurricanes. *Geophysical Research Letters*, *33*(17), 1–5. https://doi.org/10.1029/2006GL026267

Zishka, K., & Smith, P. (1980). The Climatology of Cyclones and Anticyclones over North America and Surrounding Ocean Environs for January and July, 1950–1977. *Monthly Weather Review*, *108*(4), 387–401.